

**Large- $N_C$  properties of the  $\rho$  and  $f_0(600)$  mesons from unitary resonance chiral dynamics**J. Nieves,<sup>1</sup> A. Pich,<sup>2,3</sup> and E. Ruiz Arriola<sup>4</sup><sup>1</sup>*Instituto de Física Corpuscular (IFIC), Centro Mixto Universidad de Valencia—CSIC, Edificio de Institutos de Investigación de Paterna, Aptdo. 22085, 46071, Valencia, Spain*<sup>2</sup>*Departamento de Física Teórica and IFIC, Centro Mixto Universidad de Valencia—CSIC, Edificio de Institutos de Investigación de Paterna, Aptdo. 22085, 46071, Valencia, Spain*<sup>3</sup>*Physik-Department and TUM Institute for Advanced Study, Technische Universität München, D-85748 Garching, Germany*<sup>4</sup>*Departamento de Física Atómica, Molecular y Nuclear and Instituto Carlos I de Física Teórica y Computacional, Universidad de Granada, E-18071 Granada, Spain*

(Received 19 July 2011; published 4 November 2011)

We construct  $\pi\pi$  amplitudes that fulfill exact elastic unitarity, account for one-loop chiral perturbation theory contributions and include all  $1/N_C$  leading terms, with the only limitation of considering just the lowest-lying nonet of exchanged resonances. Within such a scheme, the  $N_C$  dependence of  $\sigma$  and  $\rho$  masses and widths is discussed. Robust conclusions are drawn in the case of the  $\rho$  resonance, confirming that it is a stable meson in the limit of a large number of QCD colors,  $N_C$ . Less definitive conclusions are reached in the scalar-isoscalar sector. With the present quality of data, we cannot firmly conclude whether or not the  $N_C = 3$   $f_0(600)$  resonance completely disappears at large  $N_C$  or if it has a subdominant component in its structure, which would become dominant for a number of quark colors sufficiently large.

DOI: 10.1103/PhysRevD.84.096002

PACS numbers: 11.15.Pg, 12.39.Fe, 12.39.Mk, 13.75.Lb

**I. INTRODUCTION**

Light  $J^P = 0^+$  scalar resonance properties are of great interest, since they might help to unravel details of QCD chiral symmetry breaking and confinement. Despite many theoretical efforts, the current understanding of the microscopic structure of these resonances is still far from being complete. The difficulty is triggered by the fact that scalar mesons carry vacuum quantum numbers, and also because strong final-state interactions hide their underlying nature when they are produced. Among other resonances, the lightest one  $f_0(600)$ , currently denoted as the  $\sigma$  meson, is an essential ingredient of the nuclear force, as anticipated long ago [1]. Its contribution to the midrange nuclear attraction provides saturation and binding in atomic nuclei. During many years, there has been some arbitrariness on the “effective” scalar meson mass and coupling constant to the nucleon, partly stimulated by lack of other sources of information. The existence of this broad low-lying state is by now out of the question; its mass and width have accurately been extracted from data analysis incorporating a large body of theoretical and experimental constraints [2–4]. The debate on the nature of the  $\sigma$  meson is nonetheless not completely over. Structures of the tetraquark or glueball type have been proposed (see e.g. Ref. [5] for a recent review and references therein). It is remarkable that such an accurately determined state is so poorly understood from the more fundamental point of view of the underlying QCD dynamics of  $N_C \times N_F$  quarks and  $N_C^2 - 1$  gluons, where  $N_C = 3$  is the number of color species and  $N_F$  is the number of flavors. To clarify the issue on the nature of the  $\sigma$  meson, it has been suggested to follow the dependence on a variable number of colors  $N_C \neq 3$  of its mass and width [6] by assuming that hadronic properties

scale similarly as if  $N_C$  was large. A prerequisite for this scaling approach to work is that at least *all leading- $N_C$*  effects are taken into account.

The limit of an infinite number of quark colors keeping  $\alpha_s N_C$  fixed ( $\alpha_s$  is the strong coupling constant), turns out to be a very useful and simplifying starting point to understand many qualitative features of the strong interaction [7,8]. While keeping essential properties of quantum chromodynamics (QCD), under the assumption of confinement, the large- $N_C$  limit provides a weak coupling regime to perform quantitative QCD studies. In this work, we are interested in describing the large- $N_C$  scaling of  $\pi\pi$  scattering and the induced large- $N_C$  behavior of two-pion resonances. At leading order in  $1/N_C$ , the meson-meson scattering amplitudes are given by sums of tree diagrams induced by the exchange of an infinite number of weakly interacting physical (stable) hadrons. Indeed, meson and glueball masses scale as  $\mathcal{O}(N_C^0)$  whereas the widths do as  $\mathcal{O}(1/N_C)$  and  $\mathcal{O}(1/N_C^2)$ , respectively. Crossing symmetry implies that this sum is the tree-level approximation to some local effective relativistically-invariant Lagrangian, which by assuming that confinement still holds at large  $N_C$ , can be rewritten in terms of mesonic fields and hence complies with quark-hadron duality. Higher-order  $1/N_C$  corrections correspond to hadronic loop diagrams and effectively restore unitarity in the timelike region.

Resonance chiral theory (R $\chi$ T) [9,10] includes the pseudo-Goldstone bosons and the resonances as dynamically active degrees of freedom of the theory. The low-energy limit of R $\chi$ T must comply with low-energy theorems based on chiral perturbation theory (ChPT) [11–13], and this property has been used to predict systematically the low energy constants (LECs) of ChPT in

terms of masses and couplings of the resonances, when integrating them out of the action, at the chiral orders  $\mathcal{O}(p^4)$  [9] and  $\mathcal{O}(p^6)$  [14]. The ChPT Lagrangian includes the octet of pseudo-Goldstone bosons, however, when extending ChPT,  $R\chi T$  incorporates the resonances as active degrees of freedom that are included in nonets, since the octet and singlet of a  $SU(N_F = 3)$  group merge into a nonet for  $N_C \rightarrow \infty$ . The ChPT Lagrangian is built using the spontaneously-broken chiral symmetry of massless QCD. The explicit symmetry breaking from nonzero quark masses and electromagnetic interactions is incorporated in exactly the same way as it happens in QCD. The nonets of resonances are added requiring the general properties and invariance under charge conjugation and parity, and the structure of the operators is determined by chiral symmetry. At first order in the  $1/N_C$  expansion, terms with more than one trace and loops are suppressed. The first property permits to postpone some terms allowed by the symmetries as subleading. However, the theory determined by just symmetries does not share yet some of the known properties of QCD at high energies or accepted from hadronic Regge phenomenology.<sup>1</sup> Further constraints on the couplings arise by matching the interpolating resonance theory at intermediate energies with asymptotic QCD at the level of Green functions and/or form factors. The application of these properties determines a series of relations between the couplings of  $R\chi T$ , reducing the number of couplings and enhancing the predictability. We remind here that QCD, besides current quark masses, has only one dimensionful parameter,  $\Lambda_{\text{QCD}}$ . Of course, there are infinitely many such short-distance constraints and hence a sufficiently large number of states may eventually be needed to avoid contradictory results [15].

A further and less trivial question is related to whether or not purely contact terms should be regarded as independent of exchange terms in the large- $N_C$  framework. Within  $\pi\pi$  scattering, this corresponds to distinguish between contact  $4\pi$  vertices and those where a resonance field propagates between  $2\pi$  states (see Fig. 1). While the large- $N_C$  expansion is expected to provide a better approximation to data in the spacelike region where unitarity does not play an active role, the approach is not specifically related to a given energy range. This means that if the tower of *all* infinitely many states is included, the question on the duality between contact and exchange terms is pertinent. However, if the exchanged resonance spectrum is truncated above a given energy, contact terms must necessarily arise to encode the explicitly disregarded high-energy contributions while still complying to the short-distance constraints [10]. The explicit values of the contact LECs depend on the

functional parametrization adopted for the resonance fields.

In the single-resonance-approximation (SRA) scheme, each infinite resonance sum is just approximated by the contribution from the lowest-lying meson multiplet with the given quantum numbers. This is meaningful at low energies where the contributions from higher-mass states are suppressed by their corresponding propagators. The SRA corresponds to work with a low-energy effective field theory below the scale of the second resonance multiplets. In this work, we will use the SRA of  $R\chi T$  to reanalyze how the  $\sigma$  and  $\rho$  properties depend on  $N_C$ , mainly based on the study of  $\pi\pi$  scattering. An early investigation was proposed in Refs. [16,17] keeping the leading  $1/N_C$  contributions but omitting the ChPT chiral logarithms. We impose leading- $N_C$  short-distance constraints, as discussed in detail in Refs. [10,18]. This turns out to be of capital importance because it leads to a clear distinction between leading and subleading  $N_C$  contributions to the  $\pi\pi$  amplitudes. It also allows for a meaningful extension of the framework to the  $N_C > 3$  world. Besides, enforcing the short-distance constraints reduces the number of free parameters to only the subtraction constants, needed to restore exact elastic unitarity, and the masses of the exchanged resonances. In addition, we check that a direct analysis of  $\pi\pi$  scattering at leading order in  $1/N_C$  and using high-energy constraints, based on forward dispersion relations and Regge phenomenology, generates relations between the resonance properties compatible with those already obtained in [10,18] by looking at other processes.

We will first construct  $\pi\pi$  amplitudes that fulfill exact elastic unitarity, account for one-loop ChPT contributions, and include all  $1/N_C$  leading terms in the SRA. Next, we will look for poles in the appropriate unphysical sheets of the amplitudes, and discuss their properties when  $N_C$  deviates from its physical value,<sup>2</sup> to learn details on their nature. In this manner, we improve on previous analyses [6,21–23] where leading  $1/N_C$  terms, beyond a certain order in the chiral expansion, were neglected.

On the other hand, in the strict chiral and large- $N_C$  limits, the pseudoscalar singlet  $\eta_1$  and the  $\pi$  are degenerate [24–26]. The interplay between ChPT and large  $N_C$  has been addressed in Ref. [27].  $U(3)$  meson-meson scattering has been treated in [28] with only contact  $\mathcal{O}(p^2)$  chiral interactions. In Ref. [29], in addition to the contact  $\mathcal{O}(p^2)$ , the leading- $N_C$  scalar resonance exchange has been included, but leaving aside the vector meson exchange. This latter mechanism not only contributes to the P-waves, but also to other S-wave channels via the left-cut contribution. Recently, a full-fledged one-loop unitarized

<sup>1</sup>Regge behavior, while not directly deduced from QCD, works rather well and has played a decisive role in the benchmark and unprecedented accurate determination of the  $\sigma$  meson mass and width [2–4], by extending the high energy region above  $\sqrt{s} > 1.4$  GeV.

<sup>2</sup>We will focus here on the properties of the poles in the complex  $s$  plane. The  $N_C$  behavior of the Breit-Wigner resonance parameters has been discussed, in a model-independent manner, at length in Refs. [19,20], and we refer the reader to this latter work for further details.



FIG. 1. Leading large- $N_C$   $\pi\pi$  scattering diagrams made of contact (polynomial) and resonance-exchange (pole) terms in  $t$ ,  $s$  and  $u$  channels.

couple-channel  $U(3)$  calculation, including both scalar and vector resonance exchanges, has been undertaken in Ref. [30]. Besides achieving an excellent description of phase shifts until center-of-mass energies of around 1.4 GeV, this reference also analyzes the  $N_C$  behavior of the amplitudes. Among other results, it is explicitly shown there that when  $N_C$  increases, the mass of the lowest eigenstate of the  $\eta_1$ - $\eta_8$  mass matrix decreases, reaching values of around twice the pion mass in the  $N_C = 30$  region. Thus, a natural question arises here, namely, do the  $\eta$ - $\eta'$  degrees of freedom play a relevant role to determine the  $N_C$  trajectory of the  $\sigma$  and  $\rho$  resonances? This is addressed also in Ref. [30], from where one might infer that this is certainly not the case. Those degrees of freedom turn out to be much more relevant in the study of the  $N_C$  dependence of masses and widths of higher resonances, as for instance the  $f_0(980)$ . We benefit here from this observation, and we will neglect  $\eta$ - $\eta'$  effects in what follows.

We should also point out that some aspects of the  $N_C \neq 3$  extension undertaken in Ref. [30] deserve discussion, and we believe they can be improved along the lines followed in this paper. In particular, the leading  $1/N_C$  contributions were not properly considered in Ref. [30]. As a consequence, we cannot firmly conclude a scenario where the  $\sigma$  moves far away in the complex plane for large  $N_C$ , as obtained in [30]. We will give some more details below Eq. (24). Note that crossing symmetry, the possible absence of an exotic isotensor ( $I = 2$ ) state and the well-established fact that the  $\rho$  width decreases with  $N_C$  imply the existence of a narrow scalar-isoscalar resonance, in the large- $N_C$  limit, with a mass comparable to that of the  $\rho$  meson [31].

The paper is organized as follows. In Sec. II, we discuss the  $\pi\pi$  scattering amplitude in the SRA of  $R\chi T$  and analyze high-energy conditions which yield to the short-distance constraints. In Sec. III, the  $\mathcal{O}(p^4)$  ChPT contributions to the  $\pi\pi$  scattering amplitude and its matching to the leading  $1/N_C$  piece are discussed. Actually, we manage to write an amplitude which is correct to  $\mathcal{O}(p^4)$  and includes, within the SRA, the leading  $\mathcal{O}(1/N_C)$  terms to all orders in the chiral expansion. However, it still needs to be unitarized before being confronted to scattering data. After unitarization, we fix our parameters in Sec. IV by fitting the  $(I, J) = (0, 0)$ ,  $(1, 1)$  and  $(2, 0)$  phase shifts in the real  $N_C = 3$  world. This complies with the determination of the  $R\chi T$  Lagrangian parameters at the leading- $N_C$  approximation. Only then do we allow ourselves to analyze the

$N_C > 3$  situation in Sec. V and the emerging picture for  $\pi\pi$  resonances as the number of colors is varied. Finally, in Sec. VI we draw the main conclusions of our work. In addition, there exist two appendices (A and B), where some relevant issues of  $\pi\pi$  scattering are addressed in order to make the paper self-contained, and where we also review some features of  $\pi\pi$  forward dispersion relations and crossing symmetry, which yield to the Adler and  $\sigma$  sum rules, keeping an eye on the large- $N_C$  expansion.

## II. $R\chi T$ AND $\pi\pi$ SCATTERING

In this section, we discuss some aspects of  $R\chi T$  which will provide some useful guidance in our analysis of the large- $N_C$  limit of  $\pi\pi$  scattering. Let us denote by  $T_{IJ}(s)$ , the projection of the  $\pi\pi$ -elastic scattering amplitude with given total isospin  $I$  and angular momentum  $J$  ( $\sqrt{s}$  is the total energy in the center-of-mass frame (c.m.)). That is, if  $T_I(s, t, u)$  stands for the amplitude with total isospin  $I$ , one has (we will use here the conventions from [32])

$$T_I(s, t, u) = \sum_{J=0}^{\infty} (2J+1) T_{IJ}(s) P_J(\cos\theta) \quad (1)$$

$$\begin{aligned} T_{IJ}(s) &= \frac{1}{2} \int_{-1}^{+1} d(\cos\theta) P_J(\cos\theta) T_I(s, t(s, \cos\theta), u(s, \cos\theta)) \\ &= -16\pi \left( \frac{\eta_{IJ}(s) e^{2i\delta_{IJ}(s)} - 1}{2i\rho(s)} \right) \end{aligned} \quad (2)$$

with  $\rho(s) = \sqrt{1 - 4m_\pi^2/s}$ , being  $m_\pi = 139.57$  MeV the pion mass, and  $P_J$  the Legendre polynomials. The inelasticity  $\eta_{IJ}(s) = 1$  for  $s < 16m_\pi^2$  and  $\eta_{IJ}(s) < 1$  for  $s > 16m_\pi^2$ . Besides,  $\delta_{IJ}$  are the phase-shift and the Mandelstam variables  $t$  and  $u$  depend on  $s$  and on  $\theta$ , the scattering angle in the c.m. frame. There exists only one independent amplitude thanks to isospin and crossing symmetries, so that one has

$$T_{I=0}(s, t, u) = \frac{1}{2} \{3A(s, t, u) + A(t, s, u) + A(u, t, s)\} \quad (3)$$

$$T_{I=1}(s, t, u) = \frac{1}{2} \{A(t, s, u) - A(u, t, s)\} \quad (4)$$

$$T_{I=2}(s, t, u) = \frac{1}{2} \{A(t, s, u) + A(u, t, s)\} \quad (5)$$

where  $A(s, t, u)$  is the  $\pi^+ \pi^- \rightarrow \pi^0 \pi^0$  amplitude.

### A. $\pi\pi$ elastic scattering amplitude in the SRA

From the lowest-order  $R\chi T$  Lagrangian [9,10], describing the couplings of the lowest-lying  $V(1^{--})$ ,  $A(1^{++})$ ,  $S(0^{++})$ , and  $P(0^{-+})$  resonance nonet multiplets to the pions, we find<sup>3</sup>

$$A^{\text{SRA}}(s, t, u) = \frac{m_\pi^2 - s}{f_\pi^2} + \frac{G_V^2}{f_\pi^4} \left[ \frac{t(s-u)}{t-m_V^2} + \frac{u(s-t)}{u-m_V^2} \right] + \frac{2}{3f_\pi^4} \frac{[c_d(s-2m_\pi^2) + 2m_\pi^2 c_m]^2}{s-m_{S_8}^2} + \frac{4}{f_\pi^4} \frac{[\bar{c}_d(s-2m_\pi^2) + 2m_\pi^2 \bar{c}_m]^2}{s-m_{S_1}^2} + \frac{8d_m^2}{f_\pi^4} \frac{m_\pi^4}{m_{P_8}^2 - m_\pi^2}. \quad (6)$$

with  $f_\pi \sim 93$  MeV, the pion decay constant. In the large- $N_C$  limit,  $|\bar{c}_d| = |c_d|/\sqrt{3}$  and  $|\bar{c}_m| = |c_m|/\sqrt{3}$ . We have specified for clarity the contributions from non-degenerate singlet,  $S_1$ , and isosinglet octet,  $S_8$ , fields. Quite generally,  $m_{S_8} - m_{S_1} = \mathcal{O}(1/N_C)$  and mixing effects have been analyzed in Refs. [33,34].<sup>4</sup> Glueball mixing within  $R\chi T$  has been discussed in Ref. [35].

Taking  $m_{S_8} = m_{S_1} = m_S$ ,  $|\bar{c}_d| = |c_d|/\sqrt{3}$  and  $|\bar{c}_m| = |c_m|/\sqrt{3}$ , we reproduce the expressions in Ref. [36]. In principle, the couplings appearing in the scattering amplitude can be determined by analyzing the decay processes  $\rho \rightarrow 2\pi$  and  $S \rightarrow 2\pi$  with  $S = \sqrt{2/3}S_1 + S_8/\sqrt{3}$ , corresponding to a  $(\bar{u}u + \bar{d}d)/\sqrt{2}$  flavor composition in the  $q\bar{q}$  picture, which yield in the chiral limit (see also Ref. [37]),<sup>5</sup>

$$\Gamma_S = \frac{3c_d^2 m_S^3}{16\pi f_\pi^4}, \quad \Gamma_V = \frac{G_V^2 m_V^3}{48\pi f_\pi^4}. \quad (7)$$

The residues of the scalar-isoscalar and the vector-isovector poles in the partial-wave amplitudes are

$$g_S = \frac{c_d m_S^2}{f_\pi^2}, \quad g_V = \frac{G_V m_V^2}{\sqrt{3} f_\pi^2}. \quad (8)$$

<sup>3</sup>Here we use the antisymmetric field formulation where the  $A$ - $\pi$  mixing is absent. Note that the axial resonance does not contribute to the elastic  $\pi\pi$  scattering amplitude. After proper incorporation of short-distance constraints, the Proca formulation using  $g_V = G_V/f_\pi$  yields the same amplitude [10].  $U(3)$  nonet resonance fields are generically parametrized as  $R = \frac{1}{\sqrt{2}} \times \sum_{i=1}^8 R_i \lambda_i + \frac{1}{\sqrt{3}} R_0$  with  $\lambda_i$  the standard Gell-Mann matrices.

<sup>4</sup>Ref. [34] finds sizeable mixing effects between the singlet and octet scalar-isoscalar mesons and identifies two possible phenomenologically acceptable scenarios for the tree-level mass eigenstates: a)  $M_L = 1.35$  GeV and  $M_H = 1.47$  GeV, or b)  $M_L = 0.985$  GeV and  $M_H = 1.74$  GeV. The light solution was less preferential at it would correspond to a case where  $f_0(980)$  would not couple to pions. Therefore in several studies the heavy solution has been adopted.

<sup>5</sup>The full expressions are  $\Gamma_S = \frac{3m_S^3}{16\pi f_\pi^4} \rho_S [c_d + (c_m - c_d) \frac{2m_\pi^2}{m_S^2}]^2$  and  $\Gamma_V = \frac{G_V^2 m_V^3}{48\pi f_\pi^4} \rho_V^3$ , where  $\rho_R = \sqrt{1 - 4m_\pi^2/m_R^2}$ .

Note that the (large- $N_C$ ) relations  $g_S^2 = 16\pi\Gamma_S m_S/3$  and  $g_V^2 = 16\pi\Gamma_V m_V$  hold in the SRA, in the chiral limit. The SRA amplitude in Eq. (6) contains too many parameters to be analyzed in full detail. In the next subsections, we will discuss a sensible way of reducing the number of couplings and masses.

After projecting onto partial waves we get for the  $(I, J) = (0, 0)$ ,  $(1, 1)$  and  $(2, 0)$  channels the following asymptotic behavior at large values of  $s$ :

$$T_{IJ}^{\text{SRA}}(s) = \lambda_{IJ} \frac{2c_d^2 + 3G_V^2 - f_\pi^2}{f_\pi^4} s + \dots, \quad \lambda_{00} = 1, \quad \lambda_{11} = \frac{1}{6}, \quad \lambda_{20} = -\frac{1}{2}. \quad (9)$$

The above behavior implies that subtractions would be necessary to make convergent a dispersion relation.<sup>6</sup> We will add subtraction constants *after* unitarization.

### B. Short-distance constraints

The short-distance constraints encompass  $R\chi T$  with proper high-energy behavior [18]. In general, they produce a set of conditions which, for a limited set of resonances and in particular in the SRA, reduce the number of independent couplings. These conditions may be overdetermined yielding at times to mutually inconsistent values, a problem which can be sidestepped by introducing more resonances. In the present case, we think it of interest to pursue such an analysis within  $\pi\pi$  scattering.

In the chiral limit, the  $t$ -channel amplitudes, see Eq. (A4), in the forward direction have the following asymptotic behavior in terms of the crossing-odd variable  $\nu = (s-u)/2$ :

$$T_{I_i=0}^{\text{SRA}}(\nu, 0) = 2 \frac{c_d^2 m_S^2 + \frac{2}{3} g_T^2 m_T^2 + G_V^2 m_V^2}{f_\pi^4} + \mathcal{O}(\nu^{-2}),$$

$$T_{I_i=1}^{\text{SRA}}(\nu, 0) = \frac{6c_d^2 - 3f_\pi^2 + 4g_T^2 + 3G_V^2}{3f_\pi^4} \nu + \mathcal{O}(\nu^{-1}), \quad (10)$$

$$T_{I_i=2}^{\text{SRA}}(\nu, 0) = 2 \frac{c_d^2 m_S^2 + \frac{2}{3} g_T^2 m_T^2 - G_V^2 m_V^2/2}{f_\pi^4} + \mathcal{O}(\nu^{-2}),$$

where we have included momentarily the tensor-meson coupling  $g_T$  and mass  $m_T$ , to be discussed below in more

<sup>6</sup>Requiring that the leading term proportional to  $\lambda_{IJ}$  vanishes would yield the relation  $2c_d^2 + 3G_V^2 = f_\pi^2$ , advocated in Ref. [37]. This would imply  $G_V \leq f_\pi/\sqrt{3}$ , giving a 30% too small  $\rho \rightarrow 2\pi$  decay width. This relation has also been found as a necessary high-energy constraint in a NLO  $R\chi T$  analysis of the vector form factor, incorporating subleading  $1/N_C$  corrections [38]. In the  $c_d = 0$  limit, it gives  $G_V = f_\pi/\sqrt{3}$ , which was also found in the study of one-meson radiative tau decays carried out in [39]. Notice however that imposing this relation is not enough to make subtractions unnecessary, because the partial waves would still grow at large values of  $s$  as  $T_{IJ}(s) \sim (m_V^2 G_V^2 / f_\pi^4) \times \log(s/m_V^2)$ .

detail. This limit is compatible with the Froissart bound, a specific merit of the antisymmetric tensor formulation [10].<sup>7</sup>

As it is discussed in Appendix A, it makes sense to divide the  $\pi\pi$  scattering amplitudes in Eq. (A5) into three pieces: i) the low-energy part which takes the form of subtraction constants and is fixed by chiral symmetry, ii) an intermediate-energy part, dominated by resonance exchange, and iii) the high-energy remainder which we expect to be responsible for the Regge behavior. Therefore, if we impose a behavior for the resonance contribution no worse than suggested by Regge theory, we obtain the constraints

$$f_\pi^2 = 2c_d^2 + \frac{4}{3}g_T^2 + G_V^2, \quad (11)$$

$$0 = 6c_d^2 m_S^2 + 4g_T^2 m_T^2 - 3G_V^2 m_V^2. \quad (12)$$

These constraints correspond to require that the  $\nu$  and the  $\nu^0$  coefficients of  $T_{l_i=1}^{\text{SRA}}$  and  $T_{l_i=2}^{\text{SRA}}$ , respectively, vanish in the large- $\nu$  regime. The second condition is less robust than the first one, attending to what it is discussed on Regge phenomenology in Appendix A. Indeed, Eqs. (11) and (12) can be also obtained from the Adler and  $\sigma$  sum rules (see discussion in Sec. A 3), in the chiral limit, using the narrow-resonance approximation of Eq. (A3) to estimate the cross sections that appear in the right-hand sides of the sum rules. Note that since we have not considered any exotic isotensor resonance, we are approximating  $\sigma_2 = 0$ .

In the absence of tensor couplings,  $g_T = 0$ , these constraints imply  $c_d = \sin\phi f_\pi/\sqrt{2}$ ,  $G_V = \cos\phi f_\pi$  and  $m_V/m_S = \tan\phi$ , where  $\phi$  is a mixing angle. The KSFR relation ( $G_V = f_\pi/\sqrt{2}$ ) requires  $\phi = \pi/4$  and hence  $m_S = m_V$ , as well as  $2c_d = \sqrt{2}G_V = f_\pi$ , implying  $\Gamma_S = 9\Gamma_V/2$ . These constraints have also been found in the algebraic chiral-symmetry approach [41–43] and can be rewritten, in terms of the decay widths, as

$$1 = \frac{\Gamma_S}{m_S} \frac{32\pi f_\pi^2}{3m_S^2} + \frac{9}{2} \frac{\Gamma_V}{m_V} \frac{32\pi f_\pi^2}{3m_V^2}, \quad 0 = \frac{\Gamma_S}{m_S} - \frac{9}{2} \frac{\Gamma_V}{m_V}, \quad (13)$$

which yield the value of the scalar mass and width to be  $m_S = 660$  MeV,  $\Gamma_S = 570$  MeV, when phenomenological values for the mass and width of the  $\rho$  meson are used. These numbers are quite sensitive to details. For instance if the KSFR set of parameters is used, one gets instead (taking as input the  $\rho$  meson mass)  $m_S = m_V = 775$  MeV,  $\Gamma_S = 9\Gamma_V/2 = 805$  MeV.

<sup>7</sup>Physical results are actually independent of the field representation. The naive exchange of Proca fields does not satisfy the Froissart bound, but after suitable polynomial subtractions to comply with the short-distance constraints, one ends up with the same amplitude [10]. Fields remain a useful framework to incorporate symmetries, see also the discussion in Ref. [40].

Of course, given the fact that the scalar turns out to be a broad resonance, it is unclear what these estimates should be compared to, since generally a resonance is characterized by the complex pole and the complex residue of the scattering amplitude. The benchmark calculation of the pole on the second Riemann sheet of the  $\pi\pi$  scattering amplitude [2,3], when written as  $s_\sigma = m_\sigma^2 - im_\sigma\Gamma_\sigma$ , yields  $m_\sigma = 347(17)$  MeV and  $\Gamma_\sigma = 690(48)$  MeV. On the other hand, the connection between the Breit-Wigner (BW) resonance parameters, defined as  $\delta(m_{\text{BW}}^2) = \pi/2$  and  $\Gamma_{\text{BW}} = 1/(m_{\text{BW}}\delta'(m_{\text{BW}}^2))$ , and the pole resonance parameters has been discussed on the light of their  $N_c$  behavior in a model-independent fashion [19], suggesting that the large shift in the mass is  $\mathcal{O}(1/N_c^2)$  and can be computed, yielding an acceptable extrapolation of  $m_{\text{BW}} \sim 700$  GeV. The recent  $\pi\pi$ -scattering analysis of Ref. [44] leads to the Breit-Wigner values  $[m_{\sigma,\text{BW}}, \Gamma_{\sigma,\text{BW}}] = [841(5) \text{ MeV}, 820(20) \text{ MeV}]$ .<sup>8</sup> The quoted errors above also account for the existing differences when UFD and CFD parameterizations [44] are used. This yields a ratio  $\Gamma_{\sigma,\text{BW}}/m_{\sigma,\text{BW}} \sim 5.0(1)\Gamma_{\rho,\text{BW}}/m_{\rho,\text{BW}}$ , which suggests a 10% accuracy of large  $N_c$  in the SRA, supporting as well the identification of the large- $N_c$  parameters with the BW ones.

### C. Higher-energy resonances

We have so far been limited to states below the  $\bar{K}K$  threshold,  $\sqrt{s} < 1$  GeV. On the other hand, Regge behavior works for  $\sqrt{s} > 1.4$  GeV. So, it is interesting to see the modifications induced by other resonances which may decay into  $2\pi$ , in the mass range  $1 \text{ GeV} < m_R < 1.4 \text{ GeV}$ , namely  $f_0(980)$ ,  $h_1(1170)$ ,  $b_1(1235)$ ,  $f_2(1275)$ ,  $f_0(1370)$  and  $\rho_1(1450)$ .

After implementing the appropriate short-distance constraints, via the Froissart bound, the inclusion of a  $2^{++}$  tensor yields a resonance amplitude [45]

$$A_T(s, t, u) = -\frac{2g_T^2}{f_\pi^4} \frac{(t-u)^2 - s^2/3}{m_T^2 - s} - \frac{4g_T^2}{f_\pi^4} \frac{(s^2 - t^2 - u^2)}{m_T^2}, \quad (14)$$

where the coupling is determined from the decay into  $\pi\pi$  in a relative D-wave yielding

$$\Gamma_T = \frac{g_T^2 m_T^3}{40\pi f_\pi^4} \rho_T^5. \quad (15)$$

The previous amplitude yields the following contributions to the  $\mathcal{O}(p^4)$  ChPT couplings [45]:  $L_1^T = L_2^T = 0$  and

<sup>8</sup>The value of the pole is  $\sqrt{s_\sigma} = 445(8) - i297(7)$  MeV, in agreement with Ref. [2]. On the other hand, the model-independent large- $N_c$ -based extrapolation from the resonance pole mass to the BW pole mass [19] yields  $m_{\sigma,\text{BW}} = 670(20)$  MeV, when the UFD parameterization of Ref. [44] is used.

$L_3^T = g_T^2/(3m_T^2) \sim 0.16 \times 10^{-3}$  (see also Ref. [46]). The axial  $1^{+-}$  mesons, such as  $h_1(1170)$  and  $b_1(1235)$ , give just a purely polynomial contribution to the  $\pi\pi$  scattering amplitude (without  $s$ -channel propagator poles) which cannot satisfy the Froissart bound, yielding to no contribution at all to the LECs. We remind that the exchange of  $J > 1$  resonances in the  $t$ -channel naively violates the Froissart bound, a situation which has been the standard motivation to rely on high-energy Regge behavior as a way of introducing suitable cancellations.

If the tensor meson  $f_2(1275)$  is considered, we might include  $\rho' \equiv \rho_1(1450)$  and  $f_0(980)$  as well, where the decay widths into  $\pi\pi$  are taken to be  $\Gamma(f_2 \rightarrow \pi\pi) = 150$  MeV,  $\Gamma(f_0 \rightarrow \pi\pi) = 80$  MeV and  $\Gamma(\rho' \rightarrow \pi\pi) = 250$  MeV (note the large inaccuracies). This yields the extended sum rules (we remain in the chiral limit)

$$\begin{aligned} 1 &= \sum_S \frac{\Gamma_S}{m_S} \frac{32\pi f_\pi^2}{3m_S^2} + \sum_V \frac{9}{2} \frac{\Gamma_V}{m_V} \frac{32\pi f_\pi^2}{3m_V^2} + \sum_T 5 \frac{\Gamma_T}{m_T} \frac{32\pi f_\pi^2}{3m_T^2}, \\ 0 &= \sum_S \frac{\Gamma_S}{m_S} + \sum_T 5 \frac{\Gamma_T}{m_T} - \sum_V \frac{9}{2} \frac{\Gamma_V}{m_V}. \end{aligned} \quad (16)$$

Using PDG values [47], the higher resonances  $f_0(980)$ ,  $f_2(1275)$  and  $\rho_1(1450)$  produce corrections of the order of (0.06,  $-0.01$ ) for the rhs of the first and second sum rules, respectively. This shows a trend to cancellation which supports that higher states not only play a minor role at low energies but also in the region of interest below 1 GeV, to leading order in  $N_C$ . Therefore we will carry our analysis below with just scalar  $0^{++}$  and vector  $1^{--}$  states.<sup>9</sup>

#### D. Other short-distance constraints

Alternatively to the previous analysis, one may derive short-distance constraints from other processes involving two- and three-point functions [10,14]. Imposing the short-distance properties of the underlying QCD dynamics, within the SRA, one gets [9,18]

$$\sqrt{2}G_V = 2c_d = 2c_m = 2\sqrt{3}\bar{c}_d = 2\sqrt{3}\bar{c}_m = 2\sqrt{2}d_m = f_\pi. \quad (17)$$

These constraints are obtained from a variety of processes, some of them involving electroweak probes. It is remarkable that they turn out to be totally compatible with those deduced here by looking to  $\pi\pi$  phenomenology at high energies, for a vanishing tensor-meson contribution

<sup>9</sup>Of course, it is intriguing to analyze the role of the  $(I^G, J^{PC}) = (2^+, 0^{++})$  exotic state, named X(1420) in the PDG [47] (and found also in the SU(6) study of Ref. [48]), which decays into  $2\pi$  in a S-wave with estimated mass  $M_X = 1420(20)$  MeV and width  $\Gamma_X = 160(20)$  MeV. The contributions of such a state to the Adler and  $\sigma$  sum rules, Eqs. (A16) and (A17), in the narrow-resonance approximation are  $-80\pi\Gamma_X/3m_X^3 \sim -4.6$  GeV<sup>-2</sup> and  $16\pi\Gamma_X/3m_X \sim 1.9$ , respectively. As compared to the individual contributions from other mesons, they seem too small to provide a clear signal.

( $g_T = 0$ ). Neglecting the  $f_2(1270)$  and higher-mass resonance contributions leads to a realistic and simplified scenario for the purpose of the present work. On the other hand, from the  $\pi\pi$  scattering amplitude, we have derived the additional restriction  $m_S = m_V$ . Although we will explore the effects of this constraint in one of the fits that will be presented below, we should mention here that it relies on the assumption of an asymptotic behavior for  $T_{I=2}(\nu)$  more convergent than that of a constant ( $\nu^0$ ). This is not a totally robust result, though it is certainly plausible, given the accuracy of current  $\pi\pi$  analyses at high energies [44].

For  $m_V = 775$  GeV, the conditions in Eq. (17) lead to

$$\begin{aligned} \Gamma_S &= \frac{3m_S^3}{64\pi f_\pi^2} \rho_S = 750 \text{ MeV}, \\ \Gamma_V &= \frac{m_V^3}{96\pi f_\pi^2} \rho_V^3 = 150 \text{ MeV}. \end{aligned} \quad (18)$$

Besides, by requiring the two-point correlation functions of two scalar or two pseudoscalar currents to be equal at high energies, up to corrections of the order  $\alpha_s f^4/t^2$ , one finds [18]  $m_{p_8} = \sqrt{2}m_S$ . This relation involves a small correction, of the order 5%, which we neglect, together with the tiny effects from light quark masses. We will use Eq. (17) to fix our parameters below, and allowing  $m_S$  to be different from  $m_V$ .

### III. ONE-LOOP CHPT CORRECTIONS, UNITARIZATION OF THE $\pi\pi$ ELASTIC SCATTERING AMPLITUDE AND LARGE- $N_C$ COUNTING RULES

#### A. $\pi\pi$ scattering at one loop in ChPT

At  $\mathcal{O}(p^4)$  in ChPT, the  $\pi\pi$  elastic scattering amplitudes can be written in the form [12]:

$$A^{\text{ChPT}}(s, t, u) = A_2^{\text{ChPT}}(s, t, u) + A_4^{\text{ChPT}}(s, t, u), \quad (19)$$

$$A_2^{\text{ChPT}}(s, t, u) = \frac{m_\pi^2 - s}{f_\pi^2}, \quad (20)$$

$$\begin{aligned} A_4^{\text{ChPT}}(s, t, u) &= \frac{-1}{96\pi^2 f_\pi^4} \left\{ (2\bar{l}_1 + \bar{l}_2 - \frac{7}{2})s^2 + \left( \bar{l}_2 - \frac{5}{6} \right) (t-u)^2 \right. \\ &\quad + 4 \left( 3\bar{l}_4 - 2\bar{l}_1 - \frac{1}{3} \right) m_\pi^2 s \\ &\quad - \left( 3\bar{l}_3 + 12\bar{l}_4 - 8\bar{l}_1 - \frac{13}{3} \right) m_\pi^4 \\ &\quad + 3(s^2 - m_\pi^4) \bar{J}(s) + (t(t-u) - 2m_\pi^2 t \\ &\quad + 4m_\pi^2 u - 2m_\pi^4) \bar{J}(t) + (u(u-t) \\ &\quad \left. - 2m_\pi^2 u + 4m_\pi^2 t - 2m_\pi^4) \bar{J}(u) \right\}. \end{aligned} \quad (21)$$

The lowest-order amplitude  $A_2^{\text{ChPT}}(s, t, u)$  is identical to the first term in Eq. (6) (pion contribution) and only depends on the pion mass and weak decay constant. The  $\mathcal{O}(p^4)$

correction involves four SU(2) renormalization-scale-independent LECs:  $\bar{l}_i$  ( $i = 1, 2, 3, 4$ ). In addition,  $A_4^{\text{ChPT}}(s, t, u)$  includes one-loop chiral corrections, which are suppressed by one power of  $1/N_c$ ; they are parameterized through the loop function

$$\bar{J}(s) = 2 + \rho(s) \log \left[ \frac{\rho(s) - 1}{\rho(s) + 1} \right]. \quad (22)$$

The relation between the LEC's  $\bar{l}_i$  and the most common SU(3) parameters  $L_i^r(\mu)$  [12,13] can be found in Appendix B.

### B. $\mathcal{O}(p^4)$ ChPT-improved SRA amplitudes and large- $N_c$ counting rules

In the limit of a large number of colors [7,8],  $A^{\text{SRA}}$  in Eq. (6) scales like  $1/N_c$ , since the pion weak decay constant behaves like  $\mathcal{O}(\sqrt{N_c})$ . Furthermore,  $A^{\text{SRA}}$  provides the leading- $N_c$  prediction for the actual  $\pi\pi$  scattering amplitude, with the only limitation of considering just the lowest-lying nonet of exchanged resonances [9]. This latter approximation is justified as long as  $s$ ,  $t$  and  $u$  are kept far from the second resonance region.

The lightest resonances have an important impact on the low-energy dynamics of the pseudoscalar bosons. Below the resonance mass scale, the singularity associated with the pole of a resonance propagator is replaced by the corresponding momentum expansion; therefore, the exchange of virtual resonances generates derivative Goldstone couplings proportional to powers of  $1/m_R^2$ . At lowest order in derivatives, this gives the large- $N_c$  predictions for the  $\mathcal{O}(p^4)$  ChPT couplings [9]. At  $\mathcal{O}(p^4)$  the amplitude  $A^{\text{SRA}}$  in Eq. (6) reduces to

$$\begin{aligned} A_4^{\text{SRA}}(s, t, u) = & \frac{m_\pi^2 - s}{f_\pi^2} - \frac{G_V^2}{f_\pi^4} \left[ \frac{t(s-u)}{m_V^2} + \frac{u(s-t)}{m_V^2} \right] \\ & - \frac{2}{3f_\pi^4} \frac{[c_d(s-2m_\pi^2) + 2m_\pi^2 c_m]^2}{m_{S_8}^2} - \frac{4}{f_\pi^4} \\ & \times \frac{[\bar{c}_d(s-2m_\pi^2) + 2m_\pi^2 \bar{c}_m]^2}{m_{S_1}^2} + \frac{8d_m^2}{f_\pi^4} \frac{m_\pi^4}{m_{P_8}^2}, \end{aligned} \quad (23)$$

which constitutes the leading  $1/N_c$  approximation to  $A^{\text{ChPT}}$ . SRA predictions for the SU(3) LEC's  $L_i(\mu)$  can be read off from the above equation, and they are explicitly given in Appendix B.

Let us pay now some attention to the  $N_c$  dependence of the one-loop ChPT amplitude. Note that from Eq. (21), the logarithmic contribution to  $A_4^{\text{ChPT}}$  scales as  $1/N_c^2$ , while the polynomial piece behaves as  $1/N_c$  in the  $N_c \gg 1$  limit. This is because, as shown in the relations (B5), the LECs  $L_i$  behave as  $\mathcal{O}(N_c)$ , with the exceptions of  $L_2 - 2L_1$ ,  $L_4$  and  $L_6$  that scale as  $\mathcal{O}(N_c^0)$  [13]. The renormalization scale dependence of the LECs provides further subleading contributions in the  $1/N_c$  counting. Unfortunately,

the measured values of the  $L_i$  couplings cannot be phenomenologically split into their large- $N_c$  leading and subleading parts. In general, one has the scale-dependent relation

$$L_i^r(\mu) = A_i N_c + B_i(\mu), \quad (24)$$

where  $A_i$  is scale independent. Note that only the  $N_c = 3$  combination is experimentally accessible. However a meaningful extension of the chiral amplitudes to an arbitrary number of colors requires some knowledge of the coefficients  $A_i$  and  $B_i$ . This difficulty is precisely what  $A_4^{\text{SRA}}$  helps to overcome, and thus the SRA predictions of Eq. (B5) can be used to read off the  $A_i$  coefficients.<sup>10</sup>

In the recent work of Ref. [30], the SRA parameters  $G_V$ ,  $c_d$ ,  $c_m$ ,  $\bar{c}_d$ ,  $\bar{c}_m$ ,  $m_V$ ,  $m_{S_8}$  and  $m_{S_1}$  are fitted to data. Afterwards and to extrapolate to  $N_c > 3$ , the resonance masses are kept constant, while all the couplings are scaled by a  $\sqrt{N_c/3}$  factor. This does not take into account that singlet and octet scalar resonances become degenerate in the large- $N_c$  limit. On the other hand, if one fits the resonance couplings to data, the fitted values do not necessarily match their leading- $N_c$  values in Eq. (17) and might incorporate some significant  $1/N_c$  subleading contributions, which later on however, are scaled as if they were leading in the  $N_c$  counting. For instance, in Ref. [30] a value of around 15 MeV is found for  $c_d$ , which is around a factor three smaller than that of  $f_\pi/2$  quoted in Eq. (17). A proper extension of this parameter when  $N_c$  deviates from 3 should be  $2c_d = f_\pi^{N_c=3} \times \sqrt{N_c/3} + (30 \text{ MeV} - f_\pi^{N_c=3})$ , instead of that assumed in [30]. For other parameters, there exist also large deviations between the fitted values found in [30] and the leading- $N_c$  estimates given in Eq. (17). These differences seem to indicate  $1/N_c$  corrections to the resonance parameters which are much larger than expected. One might wonder the underlying origin of these disturbing large deviations. The fitting strategy certainly might play some role on this; for instance, the choice of the upper energy limit or the choice of the unitarization procedure. This latter issue has some relevance which we will address now. In the next section, we will discuss our unitarization procedure, which is rather similar to that used in Ref. [30]. There appear independent subtraction constants for each of the  $(I, J) = (0, 0)$ ,  $(1, 1)$  and  $(2, 0)$  sectors [32,50]. However, in Ref. [30], all three subtraction constants were forced to be equal. From the discussion in [32,50], this is somehow an arbitrary choice. The lack of flexibility of data fits incorporating such constraint might

<sup>10</sup>Actually, the SU(2) scale-independent LECs defined by Eq. (B1) display the  $N_c$  separation in a scale-independent fashion, since  $\bar{l}_i = a_i N_c + b$  where  $b$  is *common* to all coefficients and stems from pion loops. This allows to build differences,  $\bar{l}_i - \bar{l}_j = (a_i - a_j) N_c$ , which can be used to extract the leading- $N_c$  contributions from data up to a constant. This is illustrated in quark model calculations [49].

influence the actual values determined for the resonance couplings and their estimated scaling with  $N_C$ .

Let us come back to our scheme. The amplitude  $A_4^{\text{SRA}}$  in Eq. (23) contains neither pion loop terms, nor the  $1/N_C$  subleading contributions to the polynomial piece of the one-loop ChPT amplitude. Thus, and to better describe the experimental phase shifts for  $N_C = 3$ , we propose to use

$$A^{\text{SRA+ChPT}}(s, t, u) = \underbrace{A^{\text{SRA}}(s, t, u)}_{\mathcal{O}(1/N_C)} + \underbrace{[A^{\text{ChPT}}(s, t, u) - A_4^{\text{SRA}}(s, t, u)]}_{\mathcal{O}(1/N_C^2)}. \quad (25)$$

In this way, by construction, we recover the one-loop ChPT results, while at the same time all terms in the amplitude that scale like  $1/N_C$  (leading) are also included within the SRA. Note that in the  $1/N_C$  counting, the correction  $\{A^{\text{ChPT}}(s, t, u) - A_4^{\text{SRA}}(s, t, u)\}$  is incomplete since it does not account for all existing subleading  $1/N_C^2$  contributions to  $A(s, t, u)$ . A complete  $1/N_C^2$  calculation would require quantum corrections stemming also from the low-lying resonances [38,51–55].

### C. Unitarized amplitudes

The ChPT loops incorporate the unitarity field theory constraints in a perturbative manner, order by order in the chiral expansion. Though subleading in the  $1/N_C$  counting, their effect appears to be crucial for a correct understanding of  $S$ -wave  $\pi\pi$  phase shifts. Furthermore, resonances show up as poles of the unitarized amplitudes in unphysical sheets, which positions provide their masses and widths. Thus, to discuss the nature of the  $f_0(600)$  resonance, it is crucial to restore unitarity. Any unitarization method resums a perturbative expansion of the scattering amplitude in such a way that two-body elastic unitarity,

$$\text{Im} T_{IJ}^{-1}(s) = \frac{\rho(s)}{16\pi}, \quad s > 4m_\pi^2, \quad (26)$$

is implemented exactly. To restore unitarity, we will make use here of a once-subtracted dispersive representation of  $T_{IJ}^{-1}(s)$  (see for instance Sec. 6 of Ref. [32]). Let be  $\mathcal{T}_{IJ}^{\text{SRA+ChPT}}(s)$  and  $[T_2]_{IJ}(s)$ , the  $\pi\pi$  amplitudes, in the  $(I, J)$  sector, deduced from  $A^{\text{SRA+ChPT}}(s, t, u)$  and  $A_2^{\text{ChPT}}(s, t, u)$ , respectively. We define an unitarized amplitude as [32]

$$T_{IJ}^{-1}(s) = -C_{IJ} - \bar{I}_0(s) + V_{IJ}^{-1}(s), \quad (27)$$

$$V_{IJ}(s) = \mathcal{T}_{IJ}^{\text{SRA+ChPT}}(s) - [T_2]_{IJ}(s)(\bar{I}_0(s) + C_{IJ})[T_2]_{IJ}(s), \quad (28)$$

where  $V_{IJ}$  stands for the two-particle irreducible amplitude, and the subtraction constant and the loop function are given by

$$C_{IJ} = -T_{IJ}^{-1}(4m_\pi^2) + V_{IJ}^{-1}(4m_\pi^2), \quad (29)$$

$$\bar{I}_0(s) = \frac{1}{16\pi^2}[2 - \bar{J}(s)].$$

Note that i) the constants  $C_{IJ}$  determine the scattering length/volume in each sector and become undetermined free parameters, and ii) with the election of  $V_{IJ}^{-1}(s)$ , and considering  $A^{\text{SRA}}(s, t, u) - A_4^{\text{SRA}}(s, t, u)$  as  $\mathcal{O}(p^6)$ , we recover from  $T_{IJ}(s)$  the ChPT series up to one loop, in all  $(I, J)$  sectors.

Analytical expressions for the ChPT amplitudes projected onto the different  $(I, J)$  sectors can be found in the appendix B of Ref. [32].

A final remark concerning the  $1/N_C$  counting rules is in order here. The subtraction constants  $C_{IJ}$  must scale as

$$C_{IJ} \sim \mathcal{O}(N_C^0), \quad (30)$$

because of their definition as the difference between the inverses of the full and the two-particle-irreducible amplitudes at threshold for each  $(I, J)$  sector.<sup>11</sup> Thus, the amplitude  $T_{IJ}(s)$  reduces to the  $1/N_C$  leading part of  $\mathcal{T}_{IJ}^{\text{SRA+ChPT}}(s)$  in the limit of a large number of colors.

### IV. $N_C = 3$ PHASE SHIFTS AND $\rho$ AND $f_0(600)$ MESON PROPERTIES

In this section, we fit the  $C_{IJ}$  parameters to phase-shift data and show results for the poles found in the second Riemann sheet (SRS) of the amplitudes. The SRS of the  $T$  matrix is determined by the definition of the loop function  $\bar{I}_0(s)$  in the SRS. We follow here Ref. [56] and use Eq. (A13) of this latter reference to compute  $\bar{I}_0(s)$  in the SRS.<sup>12</sup>

Masses and widths of the dynamically generated resonances are determined from the positions of the poles,  $s_R$ , in the SRS of the corresponding scattering amplitudes in the complex  $s$  plane, namely  $s_R = M_R^2 - iM_R\Gamma_R$ . For narrow resonances ( $\Gamma_R \ll M_R$ ),  $\sqrt{s_R} \sim M_R - i\Gamma_R/2$  constitutes a good approximation.<sup>13</sup>

The coupling constants of each resonance to the pion pair are obtained from the residues at the pole, by matching the amplitudes to the expression

<sup>11</sup>The full and the two-particle-irreducible amplitudes differ by terms which always contains at least one  $s$ -channel pion loop, which is subleading in the  $1/N_C$  power counting. Thus, the difference  $T^{-1} - V^{-1}$  scales as  $\mathcal{O}(N_C^0)$ , as one readily deduces by noting that both  $TV$  and  $(T - V)$  scale as  $\mathcal{O}(1/N_C^2)$  in the  $N_C \gg 1$  limit.

<sup>12</sup>Note that the function  $\bar{J}_0(s)$ , defined in Eq. (A8) of [56], reduces to  $\bar{I}_0(s)$  for equal masses.

<sup>13</sup>It has become customary to quote for the broad  $\sigma$  the number  $\sqrt{s_\sigma}$  instead of  $s_\sigma$ . Here, we will also quote  $\sqrt{s_\sigma}$ , but we will refrain from identifying  $\text{Re}\sqrt{s_\sigma}$  with the mass and  $-2\text{Im}\sqrt{s_\sigma}$  with the width of the resonance. For the  $\rho$  meson, the narrow-resonance approximation works within two standard deviations.

$$T_{SRs}^{IJ}(s) = \frac{g_R^2}{(s - s_R)}, \quad (31)$$

for values of  $s$  close to the pole. The couplings  $g_R$  are complex in general, and represent independent information from the pole  $s_R$ . In the narrow-resonance approximation, the extrapolation of Eq. (31) to the real axis takes a Breit-Wigner form to comply with unitarity and hence  $g_R^2 = 16\pi m_R \Gamma_R / \rho(m_R^2)$ .

The first issue is to select the set of data points to be fitted. We will consider the scalar-isoscalar, vector-isovector and scalar-isotensor elastic  $\pi\pi$  phase shifts, with a total of 107 data points, as follows.

- (i)  $I = J = 0$  sector: As our main input, we will use the Roy equations results from Refs. [3,57,58] in the energy range  $\sqrt{s} \leq 750$  GeV. We take this upper c.m. energy cut to keep negligible coupled-channel  $K\bar{K}$  effects, which give rise to the  $f_0(980)$  resonance. We have considered the phase-shift determinations of Ref. [57] and that of Eq. (4.8) of Ref. [58]. For each value of  $\sqrt{s}$ , we have used as central value the average of both results, while the absolute difference between them is taken as the error for the  $\chi^2$  fit. From threshold to the upper cut of 750 MeV, we have moved up in steps of 10 MeV, which amounts to a total of 48 phase shifts to be fitted.
- (ii)  $I = J = 1$  ( $I = 2, J = 0$ ) sector: We fit to the phase shifts compiled in Refs. [59,60] ([61,62]) and consider an upper cut of  $\sqrt{s} \leq 910$  GeV (1190 MeV), which comprises a total of 38 (21) phase shifts.

An important point has been the selection of the fitting interval. Clearly, we should restrict the range to the elastic region and, in particular, below the opening of the first inelastic  $K\bar{K}$  channel. At lowest order, this effect corresponds to the two-step process  $\pi\pi \rightarrow K\bar{K} \rightarrow \pi\pi$ , which in the subthreshold region yields a real contribution to the amplitude and is  $1/N_c^2$  and  $s_{K\bar{K}}$ -suppressed. The pure elastic rescattering is just  $1/N_c^2$ -suppressed. On the other hand, corrections to the SRA due to heavier states with mass  $M$  are of  $\mathcal{O}(1/(N_c M^2))$ . Therefore we expect that, by restricting to low energies, inelastic effects can be safely included in  $1/N_c$  corrections to the LECs. In other words, we may allow  $\sqrt{s} \sim 2M_K \sim 1$  GeV without much trouble.

The second issue is to design the fit procedure. For three out of the five fits examined here, we will fix

$$m_V = 0.77 \text{ GeV}, \quad m_S = 1 \text{ GeV}. \quad (32)$$

For the fit *B.3*, we will force  $m_V = m_S$ , as suggested from our discussion of Eqs. (11) and (12), and fit the common value to data. Finally, in the fit *B.1-2* we will fix  $m_V$  to 0.77 GeV, while  $m_S$  is considered as a free parameter. We will always fit  $C_{00}$ ,  $C_{11}$  and  $C_{20}$  to data; besides those parameters,  $m_V$  and  $m_S = m_P/\sqrt{2}$ ,  $A^{\text{SRA+ChPT}}$  depends still on  $L_{1,2,3,4,5,6,8}^r(\mu)$ , once the relations in Eq. (17) are implemented.

We have considered two well-differentiated scenarios:

- (i) *A*: We just take the SU(3) Gasser-Leutwyler parameters  $L_i^r(\mu)$ , at a certain scale  $\mu$ , from other phenomenological analyses. In this type of fits, only the  $C_{IJ}$  parameters are fitted to data.
- (ii) *B*: The contributions of the low-lying vector, axial-vector, scalar and pseudoscalar resonances to the  $L_i$ , and therefore to the effective chiral Lagrangian at order  $\mathcal{O}(p^4)$ , were given in Eq. (B5), and thus, the renormalized coupling constants  $L_i^r(\mu)$  can be written as a sum [9]

$$L_i^r(\mu) = L_i^{\text{SRA}} + \hat{L}_i^r(\mu) \quad (33)$$

of the resonance contributions,  $L_i^{\text{SRA}}$  and a remainder  $\hat{L}_i^r(\mu)$ . The choice of the renormalization scale  $\mu$  is arbitrary. However, it is rather obvious that one can only expect the resonances to dominate the  $L_i^r(\mu)$  when  $\mu$  is not too far away from the resonance region. Therefore, it is common to adopt  $\mu = m_\rho$  as a reasonable choice. However, one might take as a best fit parameter one scale,  $\mu^{\text{RS}}$ , for which it occurs a complete resonance saturation of all the LECs  $L_i^r$ , this is to say

$$\hat{L}_i^r(\mu^{\text{RS}}) = 0. \quad (34)$$

In other words, at this privileged scale  $\mu^{\text{RS}}$ , there is no other contribution in addition to the meson resonances. In this type of fit, besides the  $C_{IJ}$  parameters, this scale should be fitted to data.

We have also considered a scenario where the complete resonance saturation of the LECs  $L_i^r$  occurs at two different scales,  $\mu_V^{\text{RS}}$  for  $L_{1,2}^r$  and  $\mu_S^{\text{RS}}$  for  $L_{4,5,6,8}^r$ , depending whether the LEC is dominated by the vector or the scalar resonance contribution. Note that,  $L_3$  is renormalization-scale invariant.

Let us start discussing results obtained from five different fits to the phase-shift data. Best fit parameters and pole properties are compiled in Table I, while predicted phase shifts are depicted in Fig. 2. We have checked that none of the fits give rise to spurious poles on the real axis below and close to the  $\pi\pi$  threshold. Indeed, we have looked for poles down in the real axis to  $s \sim -(0.65 \text{ GeV})^2$  and have not found any one.

In the first fit (*A*), we take the SU(3) Gasser-Leutwyler parameters  $L_i^r(\mu = m_\rho)$  from the  $\mathcal{O}(p^4)$   $K_{\ell 4}$  fit compiled in Table 2 of Ref. [63].<sup>14</sup> A best fit to data using, instead, the central values of the main  $\mathcal{O}(p^6)$  fit of Ref. [63] leads to a  $\chi^2/\text{dof}$  more than twice larger than that of fit *A*. This is not entirely surprising, since we are only considering here one-loop chiral logarithms, besides those required to

<sup>14</sup>In units of  $10^{-3}$ ,  $L_{1,2,3,4,5,6,8}^r(\mu = m_\rho) = 0.46, 1.49, -3.18, 0., 1.46, 0.$  and  $1.08$ , respectively. For simplicity in the analysis, we have ignored the errors on these parameters, since they do not affect the main conclusions of this work.

TABLE I. Best fit parameters and pole properties (statistical uncertainties on these latter quantities define 68% confidence-level regions, induced by the corresponding Gaussian correlated errors of the different fit parameters). The three  $C_{IJ}$  parameters are always fitted to data, and in addition  $\mu_V = \mu_S$ ,  $\mu_V$  and  $\mu_S$ ,  $\mu_S$  and  $m_S$ , and  $\mu_V = \mu_S$  and  $m_V = m_S$  are also adjusted in the case of fits  $B.1$ ,  $B.2$ ,  $B.1-2$  and  $B.3$ , respectively. In the row labeled as *contrb.*, the contributions to the  $\chi^2$  of the different ( $I = J = 0$ )/( $I = J = 1$ )/( $I = 2, J = 0$ ) sectors are displayed. Besides,  $r_{ij}$  are Gaussian correlation coefficients between parameters  $i$  and  $j$ . Note that the dispersive data analyses based in Roy [2] and GKPY [4] equations predict for  $\sqrt{s_\sigma} = (441_{-8}^{+16}, -i272_{-12}^{+9})$  MeV and  $(457_{-13}^{+14}, -i279_{-7}^{+11})$  MeV respectively, while the Review of Particle Properties [47] quotes  $m_\rho = 775.49 \pm 0.34$  GeV and  $\Gamma_\rho = 149.1 \pm 0.8$  GeV.

	A	B.1	B.2	B.1-2	B.3
$C_{00}$	-0.0210 (5)	-0.0218 (9)	-0.0278 (18)	-0.0283 (18)	-0.0142 (4)
$C_{11}$	-0.02054 (11)	-0.01996 (11)	-0.01979 (12)	-0.01968 (12)	-0.0109 (9)
$C_{02}$	-0.0594 (19)	-0.0588 (20)	-0.0621 (17)	-0.0593 (19)	-0.0602 (18)
$\mu_V^{RS}$ (MeV)	770 (fixed)	693 (26)	474 (16)	693 (fixed B.1)	546 (22)
$\mu_S^{RS}$ (MeV)	770 (fixed)	$\mu_V^{RS}$	1550 (180)	1190 (130)	$\mu_V^{RS}$
$m_S$ (MeV)	1000 (fixed)	1000 (fixed)	1000 (fixed)	1295 (40)	739 (3)
$m_V$ (MeV)	770 (fixed)	770 (fixed)	770 (fixed)	770 (fixed)	$m_S$
$\chi^2/\text{dof}$	3.5	2.4	2.0	2.0	2.2
contrb. $\chi^2$	25/323/21	26/203/22	5/178/20	17/171/20	17/192/20
$r_{12}, r_{13}, r_{14}, r_{15}$	0, 0, -, -	0.06, 0.13, 0.80, -	0.04, 0.05, 0.43, 0.20	0.09, -0.01, 0.47, -0.05	0.20, 0.08, 0.52, -0.19
$r_{23}, r_{24}, r_{25}$	0, -, -	0.01, 0.07, -	-0.02, -0.12, 0.21	-0.01, 0.29, 0.27	-0.02, -0.19, -0.99
$r_{34}, r_{35}$	-, -	0.06, -	0.14, -0.10	-0.03, -0.03	0.05, 0.02
$r_{45}$	-	-	-0.59	0.60	0.21
$m_\rho$ (MeV)	749.1 (4)	752.6 (5)	754.0 (5)	754.8 (6)	754.7 (7)
$\Gamma_\rho$ (MeV)	144.5 (3)	150.4 (4)	152.0 (4)	153.1 (5)	149.5 (4)
$ g _\rho$ (MeV)	2404 (4)	2490 (5)	2515 (5)	2534 (7)	2504 (6)
$\sqrt{s_\sigma}$ (MeV)	$(451 \pm 2,$ $-i234 \pm 1)$	$(453 \pm 4,$ $-i238 \pm 4)$	$(423 \pm 6,$ $-i267 \pm 3)$	$(442 \pm 4, -i248 \pm 2)$	$(443 \pm 4, -i240 \pm 4)$
$ g _\sigma$ (MeV)	3005 (21)	3080 (70)	3070 (120)	3100 (50)	2990 (80)
$m_{\text{scl}}$ (MeV)	1340 (40)	$1600_{-1200}^{+0}$	772 (6)	$1020_{-650}^{+70}$	990 (30)
$\Gamma_{\text{scl}}$ (MeV)	$117_{-0}^{+22}$	$300_{-0}^{+300}$	$580_{-0}^{+120}$	$1070_{-0}^{+240}$	$170_{-0}^{+40}$
$ g _{\text{scl}}$ (MeV)	2800 (300)	$4700_{-1700}^{+0}$	2980 (100)	2940 (120)	$2900_{-300}^{+400}$

restore exact unitarity, in the  $\pi\pi$  amplitudes. In the four other fits ( $B.1$ ,  $B.2$ ,  $B.1-2$ , and  $B.3$ ), we assume that complete resonance saturation occurs, the corresponding scale (or scales) where it holds is fitted to data. In the fit  $B.1-2$ , we fix  $\mu_V^{RS}$  to the value obtained in fit  $B.1$  and we fit  $\mu_S^{RS}$  and  $m_S$  to data. Besides in the fit  $B.3$ , we force  $m_S = m_V$  in the SRA amplitude, and fit this common mass to the data. We explore this possibility because it is suggested from our previous discussion on short-distance conditions in Eqs. (11) and (12). The  $m_S = m_V$  constraint was deduced in Ref. [23] as well, when the one-loop SU(2) ChPT amplitude, unitarized with the Inverse Amplitude Method (IAM), was required to be consistent with the SRA.

Since in the SRA amplitudes we have explicitly incorporated one vector and one scalar poles, we expect at least one pole in each of the  $I = J = 0$  and  $I = J = 1$  sectors. Because of the resummation in Eq. (27), the pole positions will change with respect to those of the bare ones ( $s = m_V^2$  and  $s = m_S^2$ ) and the resonances will acquire a width that accounts for their two-pion decay. In addition, as we will see, some other poles are generated as well in the SRS of the scattering amplitudes. The five fits have reasonable values of  $\chi^2/\text{dof}$ , though in the  $I = J = 1$  channel  $B$ -type

fits lead to a better agreement with data than fit  $A$ . The major improvement occurs at the higher end of the fitted region, and it is due to the tail of a second resonance located at around 1.4 GeV that it is generated in the  $B$  schemes. The relation  $g_\rho^2 = m_\rho^4/(6f^2)$ , deduced from the KSFR prediction  $\Gamma_\rho = m_\rho^3/(96\pi f_\pi^2)$ , is satisfied within 3% accuracy. This is because the chiral logarithms are almost negligible in the  $\rho$ -meson channel, and indeed at order  $\mathcal{O}(p^4)$  they cancel out for the SU(2) massless pion theory [23].

Besides, it is also interesting to compare the leading- $N_C$  values of the residues, as displayed by Eq. (8), with the corresponding ones after unitarization, given in Table I. Using the input values one gets  $|g_V| \sim 2600$  GeV, in excellent agreement with the values for  $|g_\rho|$  quoted in the table that range in the interval 2400–2500 GeV. For the scalar resonance the rather stable values for  $|g_\sigma| \sim 3000$ –3100 GeV can only be reproduced by Eq. (8) if  $m_S = m_V$  (Fit  $B.3$ ). Indeed, for the  $B.3$  fitted  $m_S = m_V$  mass, we find  $|g_S| \sim 3000$  GeV. For completeness, let us mention that the residue of the  $\sigma$  resonance has also been deduced from the  $\sigma \rightarrow \gamma\gamma$  decay [64], yielding  $g_\sigma = 3204(28) + i1588(14)$  MeV, i.e.  $|g_\sigma| = 3580(30)$  MeV.

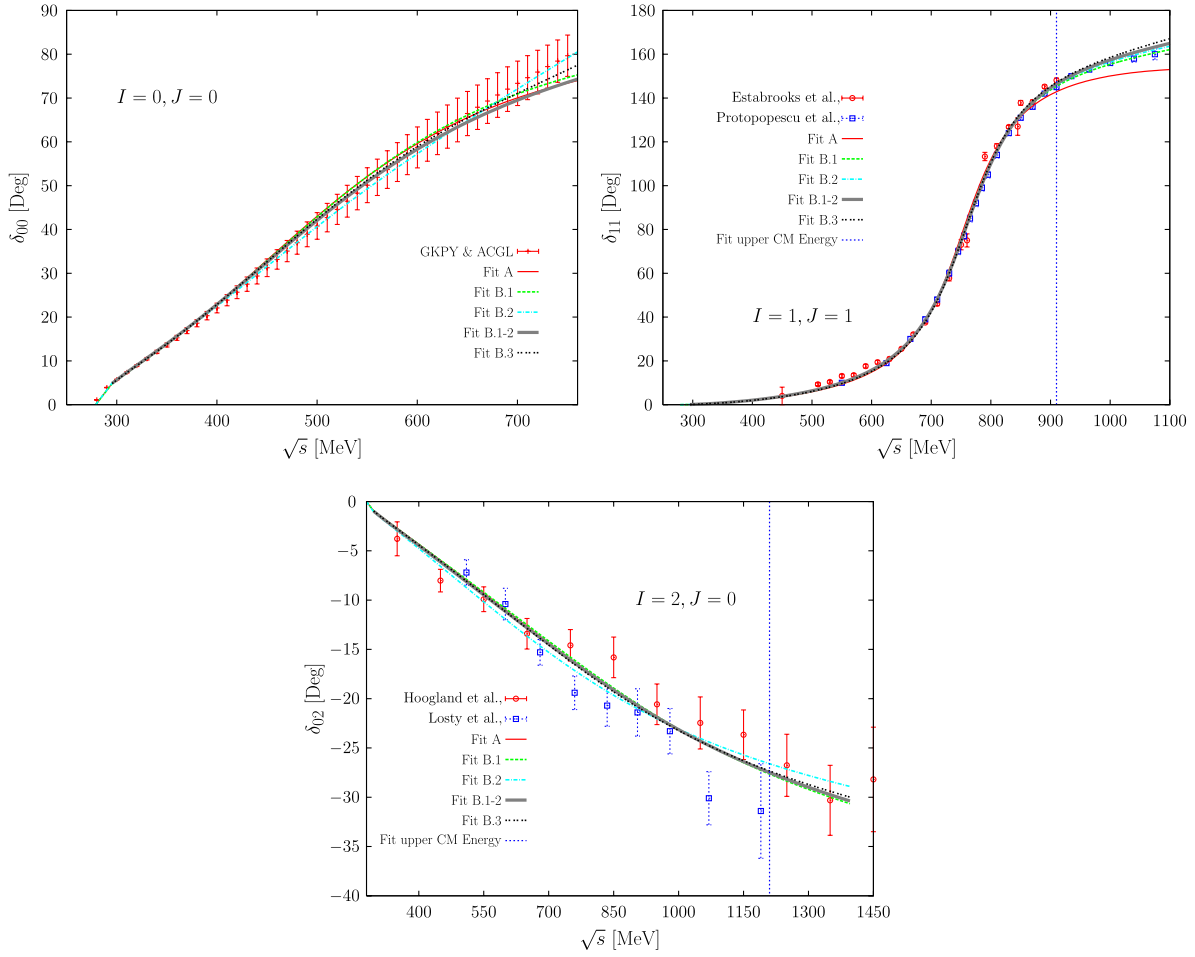


FIG. 2 (color online). Theoretical predictions for the phase shifts obtained from fits *A*, *B.1*, *B.2*, *B.1-2* and *B.3*. Fitted data from Refs. [59,60] ( $I = 1, J = 1$ ) and [61,62] ( $I = 2, J = 0$ ) are also displayed. In the isoscalar-scalar ( $I = 0, J = 0$ ) channel, the used average of the results of Refs. [57,58] is shown, as well.

The result from Roy equations yields  $|g_\sigma| = 3300(300)$  MeV [65]. Using the UFD and CFD parameterizations from [44] yields  $g_S = 3735(61) + i874(3)$  MeV and  $g_\sigma = 3742(60) + i874(6)$  MeV or, equivalently,  $|g_\sigma| = 3836(85)$  MeV and  $|g_\sigma| = 3843(84)$  MeV respectively, while in the most recent analysis based in GKPY equations, a value of  $|g_\sigma| = 3590(120)$  MeV is quoted [4].

Moreover, the scalar-isoscalar phase shifts are significantly better described when the complete resonance saturation of the  $L_i^j$  occurs at two different scales fitted to data (fit *B.2*). In this latter case, mass and width of the  $f_0(600)$  or  $\sigma$  resonance compare also well with the results of Caprini *et al.* [2].<sup>15</sup> The properties of the  $\sigma$  resonance are strongly influenced by chiral logarithms [23]. In this

<sup>15</sup>Bear in mind that in the  $I = J = 0$  sector we do not fit directly the Roy equation results of Ref. [57], used in the work of Caprini *et al.*, but rather we take an average of these results with those obtained by Yndurain and collaborators in Ref. [58]. The recent reanalysis [44] provides errors fully compatible with this assumption.

scalar-isoscalar channel, we will keep track of a second resonance, which cannot be identified with the  $f_0(600)$  and that we will label as *scl*. There exist two types of scenarios: i) for fits *A*, *B.1* and *B.3*, this second pole appears well above  $m_S$  (1 GeV for the first two fits and 0.739 GeV for the last one) and it is relatively narrow, and ii) for fits *B.2* and *B.1-2*, it is placed below  $m_S$  (1 GeV and 1.295 GeV, respectively) and it is quite wide ( $\Gamma \geq 600$  MeV). In the case of the fit *B.2*, the effects of this resonance (*scl*) on the phase shifts, in the higher end (600–750 MeV) of the fitting range, are appreciable and considerably improve the achieved description (see Fig. 2). A different question is whether or not such a wide state, below 1 GeV, does have a correspondence with any physical state or it is just an artifact of the fitting procedure. We should note that a state with these features has not been reported neither in the Roy equation analysis of Ref. [65], nor in the most recent work based in the GKPY equations of Ref. [4]. As we shall see in the next subsection, the  $N_c \gg 1$  behavior of the  $\sigma$ -pole obtained from the *B.2* fit is radically different to that inferred from the *A*, *B.1*, and *B.3* schemes. That is the

reason why we have proposed the fit *B.1-2*, with the intention of testing to what extent the dependence on  $N_C$  of the  $\sigma$ -resonance properties is determined by the existence of this possible artifact.<sup>16</sup> In the fit *B.1-2*, where the scale  $\mu_V^{RS}$  is fixed to the result of fit *B.1* and the value of  $m_S$  is adjusted to the data, the second scalar resonance shows up above 1 GeV, and as we will discuss below, it leads to qualitatively the same  $N_C$  dependence of the  $f_0(600)$  mass and width as the fit *B.2* does. Nevertheless, we should point out that the exact position and properties of the second scalar pole is not of much relevance for the present work, and we have little control on them, since they might be affected by higher energy effects (coupled channel dynamics, for instance) not considered here. However, what is relevant is that as we will show in the next section, its mere existence influences the properties of the  $f_0(600)$  resonance, when  $N_C$  deviates from 3.

### V. RESULTS FOR $N_C > 3$

We extrapolate the amplitudes to  $N_C > 3$ , by means of the  $N_C$  dependence

$$A^{\text{SRA+ChPT}}(s, t, u)|_{N_C \geq 3} = \frac{3}{N_C} A^{\text{SRA}}(s, t, u)|_{N_C=3} + \left(\frac{3}{N_C}\right)^2 \left( A^{\text{ChPT}}(s, t, u) - A_4^{\text{SRA}}(s, t, u) \right) \Big|_{N_C=3}, \quad (35)$$

and the scaling law of Eq. (30).  $N_C > 3$  results are depicted in Figs. 3–5.

In what the  $\rho$  meson properties concerns, we observe that for all five fits examined here (Fig. 3), both mass and width behave as expected from a  $q\bar{q}$  picture. Thus  $m_\rho$ , that did not deviate at  $N_C = 3$  much from  $m_V$ , quickly approaches to  $m_V$ , while  $\Gamma_\rho$  decreases like  $1/N_C$ , as the number of colors increases. This is not by any means a new result, and in the past other authors have already reached, within an unitarized ChPT scheme, this conclusion [6,22]. Indeed, in a previous work [23], the same result was obtained starting from the one-loop SU(2) ChPT amplitude for massless pions and using, as in Refs. [6,22], the IAM to restore elastic unitarity. However, results here are more robust, because in previous works the leading  $1/N_C$  terms appearing beyond  $\mathcal{O}(p^4)$  [6,23] or  $\mathcal{O}(p^6)$  [22] were simply ignored. Note that the constraint  $m_V = m_S + \mathcal{O}(1/N_C)$ , deduced in Ref. [23] when the one-loop unitarized  $\pi\pi$  amplitude was required to be consistent with the SRA, does no longer necessarily hold here, and we could still have both parameters to be independent (fits *A*, *B.1*, *B.2*,

and *B.1-2*). Though this could be because we keep here all  $1/N_C$  terms at all chiral orders, it might also happen that the above constraint was just an artifact of the IAM used in [23] to unitarize the amplitudes. Nevertheless, we should note that fit *B.3*, where the constraint  $m_V = m_S$  is enforced, leads to phenomenologically acceptable results as well.

Let us move on, and discuss now the scalar-isoscalar channel. For sufficiently large  $N_C$ , and since unitarization corrections are subleading, we should end up with just the unique resonance (of mass  $m_S$ ) included in the SRA irreducible amplitude, while the effects of the second resonance must disappear. We see in Figs. 4 and 5 that this is effectively the case. However, now it is difficult to draw robust conclusions and the resonance that survives depends on the fit procedure.

In the case of the fits *A*, *B.1*, and *B.3*, we see that the resonance identified as the  $f_0(600)$  for  $N_C = 3$  becomes the SRA pole, with mass  $m_S$  when  $N_C$  is sufficiently large. There is a first transition region for values of  $N_C$  close to 3, where both the mass and width increase with  $N_C$ , but above  $N_C = 6-8$  the resonance width starts decreasing like  $1/N_C$ , and the mass approaches to the limiting  $m_S$  value. The behavior showed in the two upper panels of Fig. 4 is almost identical to that of the right upper panel of Fig. 1 in the two-loop analysis of [22]. The authors of this latter reference conclude that in the case of the  $\sigma$  resonance, there exists a mixing with a  $q\bar{q}$  subdominant component, arising as loop diagrams become more suppressed at large  $N_C$ . The nature of the  $\sigma$  resonance in the real world ( $N_C = 3$ ) would be totally different to that of the  $\rho$  meson, being it is mostly governed by chiral logarithms stemming from unitarity and crossing symmetry [23], justifying the widely accepted nature of the  $\sigma$  as a dynamically-generated meson. However, within this scenario, for sufficiently large  $N_C > 10$ , the structure of both ( $\sigma$  and  $\rho$ ) resonances is similar. As pointed out recently in Ref. [31], this solves the seeming paradox of how a distinctive nature for the  $\rho$  and  $\sigma$  at  $N_C = 3$  is reconciled with semilocal duality at larger values of  $N_C$ . Semilocal duality requires the contribution of these two resonances to the  $\pi^+ \pi^-$  elastic cross section to cancel<sup>17</sup> “on average,” since this process is purely isospin 2 in the  $t$ -channel, and there are no isotensor resonances at low energies.

In what respects to the second resonance found in the scalar-isoscalar channel, we see in Fig. 5 that for fits *A*, *B.1*, and *B.3*, it follows a totally different pattern with increasing  $N_C$ . Indeed, it becomes wider and wider and from one value of  $N_C$  on, the pole  $s_{\text{scl}}$  turns out to be located in the third quadrant, though  $\sqrt{s_{\text{scl}}}$  still lies in the fourth quadrant, with  $\text{Re } s < 0$  (where the path integral for the resonance field would not be well defined) and its effects on the

<sup>16</sup>The minimization procedure, involving also the election of the parameters which are fitted to data, is not completely unique, and there exist obviously different local minima. Some of them might not have a proper physical interpretation. Bearing this in mind, we can not discard the existence of artifacts.

<sup>17</sup>Note however, that such a statement requires an extrapolation of the Regge behavior to somehow low energies. For that end, the authors of Ref. [31] use Regge trajectories for the variable  $(\nu - 2m_\pi^2 - t/2)$  to ensure that the imaginary part of the extrapolated Regge amplitude vanishes at threshold.

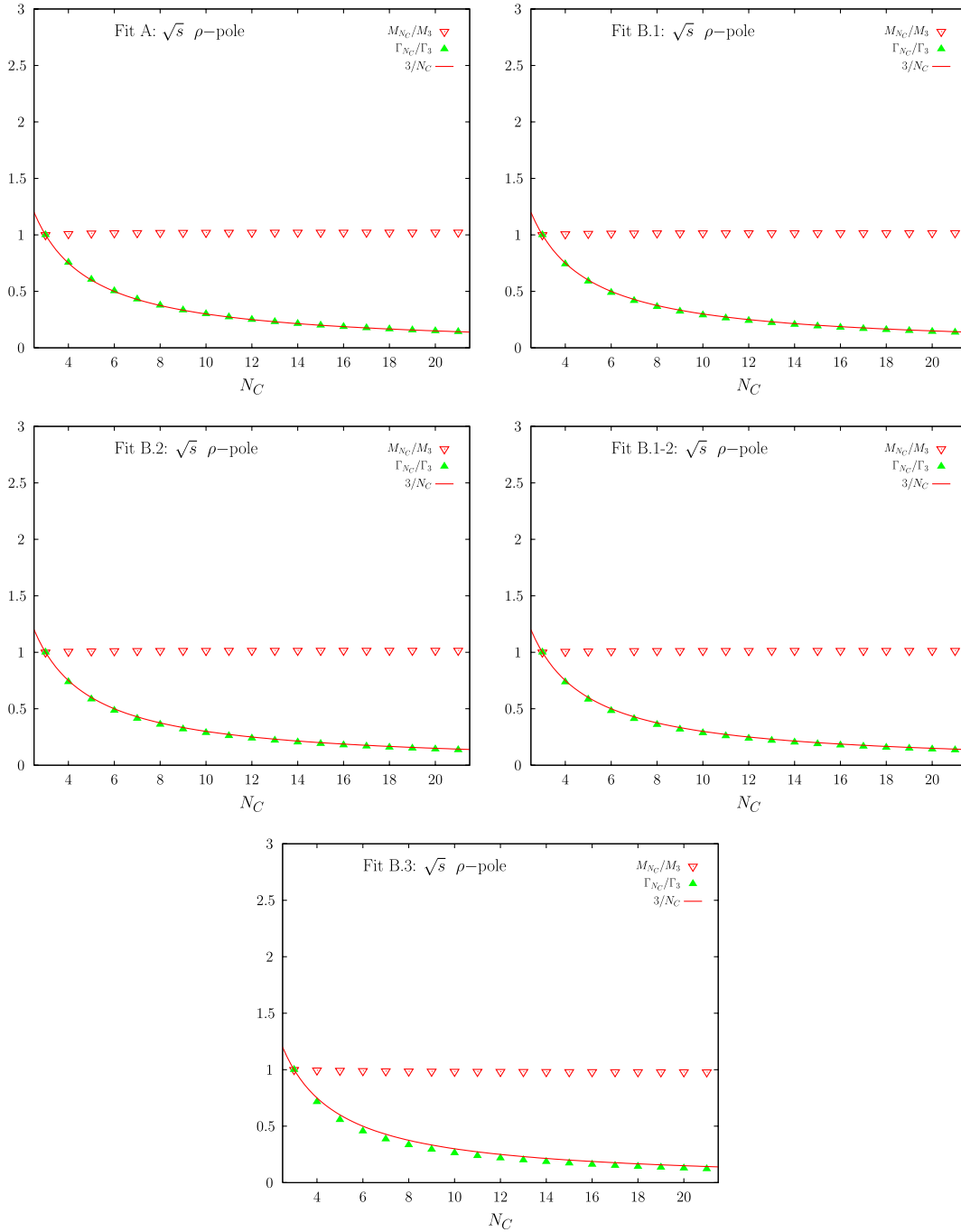


FIG. 3 (color online).  $N_c$  dependence of the  $\rho$  pole position for the various fits described in the text. Empty [filled] triangles stand for  $\text{Re}\sqrt{s_\rho}$  [ $-2\text{Im}\sqrt{s_\rho}$ ] in units of the  $N_c = 3$  values ( $M_3$  and  $\Gamma_3$ ), with  $s_\rho$  the SRS pole position (located in the fourth quadrant) for the different  $N_c$  values.

scattering disappear. We would like to mention that in Ref. [30] poles in the SRS are being searched in the variable  $\sqrt{s}$ . That could be inappropriate as we pointed out in Ref. [23], and we reiterate here. This is because, as mentioned above, there are situations where  $\sqrt{s_R}$  lies on the fourth quadrant of the SRS, but however  $s_R$  has passed to the third quadrant and thus its meaning becomes unclear. This phenomenon, which can only happen for broad

resonances, was also illustrated in Fig. 1 of [23], and it is precisely what happens for the  $\sigma$  meson case in Ref. [30] (see the Fig. 10 in that reference). The conclusion of Ref. [30] that the  $\sigma$  meson moves far away in the complex plane for large  $N_c$  overlooks the fact that it does so in the third quadrant of the complex plane.

The recent work of Ref. [66] might contradict the findings for the  $\sigma$  resonance deduced from fits A, B.1, and B.3,

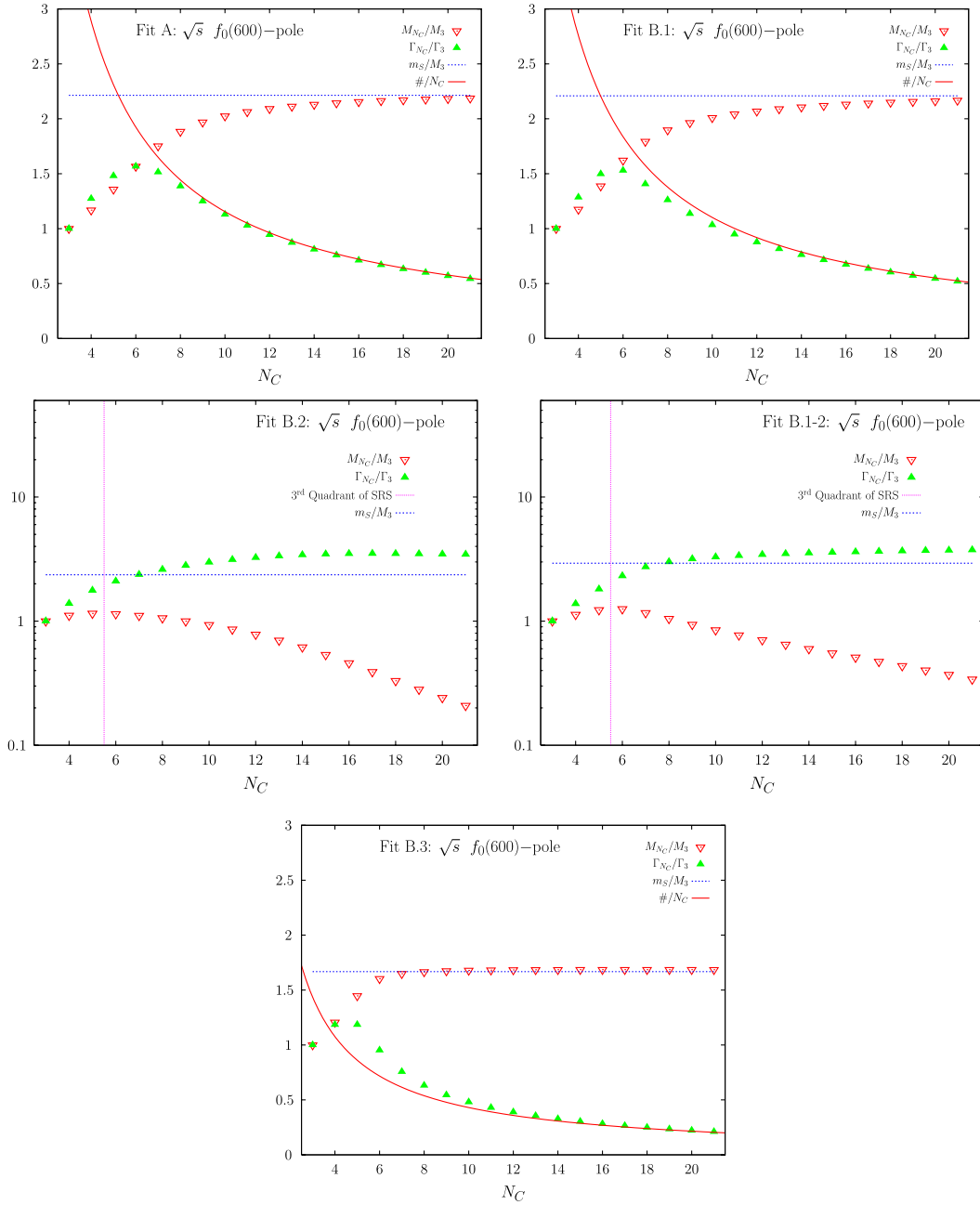


FIG. 4 (color online). Same as Fig. 3, but for the  $\sigma$  pole. In addition, the horizontal line indicates the mass of the scalar resonance included in the SRA amplitude (1 GeV for fits A, B.1 and B.2, 0.739 GeV for the fit B.3 and 1.295 GeV in the case of the fit B.1-2). For values of  $N_C$  located at the right of the vertical line in the B.2 and B.1-2 panels, the pole  $s_\sigma$  appears in the third quadrant, instead of in the fourth one, and thus the singularity does not have a clear physical interpretation.

which in turn seem compatible with those obtained in the two-loop analysis of Ref. [22]. In [66], instead, emerges a picture more consistent with that outlined in the one-loop analysis of Ref. [6]. Within the unitarized quark model proposed by Törnqvist [67], the authors of [66] find that the whole low-energy scalar spectrum below 2 GeV, except for a possible glueball  $f_0(1710)$ , could be described in one consistent picture, with the bare “ $q\bar{q}$  seeds” dressed by the hadron loops. In this model, the  $\sigma$  resonance is generated

as a pole of the  $S$  matrix and has no correspondence with any of the bare  $q\bar{q}$  seeds included in the scheme. Indeed, the  $\sigma$  resonance runs away from the real axis on the complex  $s$  plane when  $N_C$  increases. However, following Ref. [31], this scenario might not be compatible with semi-local duality, when the number of colors is sufficiently high. Besides, we should note that, in sharp contrast with the work here, it is not clear whether the  $\pi\pi$  amplitudes used in Ref. [66] contain or not all the leading  $1/N_C$

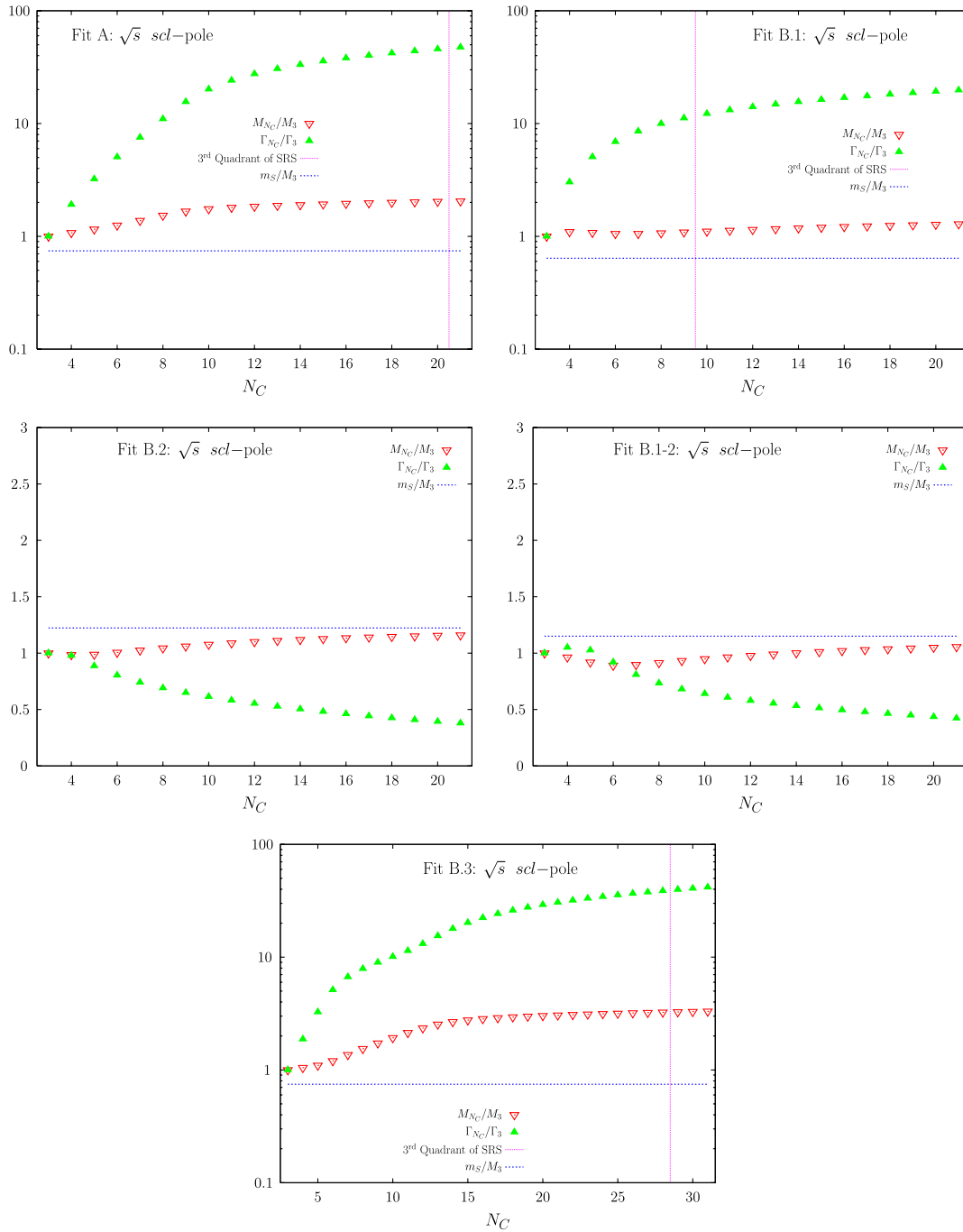


FIG. 5 (color online). Same as Fig. 3, but for the scl pole. Now, poles appear in the third quadrant for fits A, B.1 and B.3.

contributions, and thus the analysis of the behavior of the resonance properties when  $N_C$  is larger than 3 is not fully meaningful.

The qualitative  $N_C$  behavior of the two resonances found in the scalar-isoscalar sector is substantially different when one looks into the results of the fits B.2 and B.1-2 (middle panels of Figs. 4 and 5). There, the role played by the  $N_C = 3$   $\sigma$  and scl resonances is interchanged. Thus, the  $q\bar{q}$  component of the  $\sigma$  seems to be absent, and the  $f_0(600)$  pole becomes wider and moves into the third quadrant

above  $N_C > 5$ . Indeed, now the behavior showed by this pole is quite similar to that displayed for the  $\sigma$  in the right panel of Fig. 4 of Ref. [66]. On the other hand, as can be appreciated in the middle panels of Fig. 5, the second  $I = J = 0$  resonance now becomes the scalar SRA pole included in our amplitudes. Presumably, at high  $N_C$  it would become more delta-function-like, as the  $\rho$  pole would, and it would likely provide the needed cancellations with the contribution of this latter resonance in the elastic  $\pi^+\pi^-$  amplitude [31].

A recent study [68] describes an accidental symmetry of the full Regge tower of radially excited  $0^{++}$  states,  $M^2 = an + m_\sigma^2$ . Remarkably, the states generating doublets with excited pion states are  $f_0(600) \leftrightarrow \pi_0(140)$ ,  $f_0(1370) \leftrightarrow \pi_0(1300)$ ,  $f_0(1710) \leftrightarrow \pi_0(1800)$ ,  $f_0(2100) \leftrightarrow \pi_0(2070)$  and  $f_0(2330) \leftrightarrow \pi_0(2360)$ , whereas the other scalar states  $f_0(980)$ ,  $f_0(1500)$ ,  $f_0(2020)$  and  $f_0(2200)$  are not degenerate with other mesons with light  $u$  and  $d$  quarks. Arguments have been put forward to identify the  $f_0(980)$  as a would-be glueball in the large- $N_C$  limit. As it is well known, glueballs are more weakly coupled to mesons,  $\mathcal{O}(1/N_C)$ , than other mesons,  $\mathcal{O}(1/\sqrt{N_C})$ . This is supported by the rather small width ratio which yields  $\Gamma_f/\Gamma_\sigma \sim (g_{f\pi\pi}^2 m_f^3)/(g_{\sigma\pi\pi}^2 m_\sigma^3) \sim 1/N_C$ , and for  $m_\sigma \sim 0.8$  GeV a ratio  $g_{\sigma\pi\pi}/g_{f\pi\pi} \sim \sqrt{N_C}$  is obtained.

Our analysis can be improved along several lines. First, one might extend the chiral analysis to include two-loop results. Secondly, our conclusions might be modified when coupled channels incorporating  $\bar{K}K$  effects are taken into account. We have given arguments why we do not expect that this might be important as long as we remain in the subthreshold region, where all  $\bar{K}K$  effects should be included as  $1/N_C$  corrections to the counterterms.

## VI. CONCLUDING REMARKS

We summarize the conclusions of this work. First, we have constructed  $\pi\pi$  amplitudes that fulfill exact elastic unitarity, account for one-loop ChPT contributions and include all leading terms, within the SRA, in the  $1/N_C$  expansion. These amplitudes have been successfully fitted to  $I = J = 0$ ,  $I = 2$ ,  $J = 0$  and  $I = J = 1$  phase shifts. Next, we have looked for poles in the SRS of the amplitudes, and discussed their properties. Since all leading  $1/N_C$  terms are taken into account, this scheme is much more appropriated to discuss the  $N_C$  dependence of the  $\sigma$  and  $\rho$  masses and widths than previous ones, where the leading  $1/N_C$  terms appearing beyond  $\mathcal{O}(p^4)$  [6,23] or  $\mathcal{O}(p^6)$  [22] were neglected. The recent work of Ref. [30] does not identify correctly the leading  $1/N_C$  term, and hence the conclusions of this reference in the large- $N_C$  limit need some revision.

Robust conclusions are drawn in the case to the  $\rho$  resonance, and we confirm here that it is a stable meson in the large- $N_C$  limit, as pointed out by other authors in the past. In the scalar-isoscalar sector, the overall scenario looks somehow less predictive, since we cannot firmly conclude whether or not the  $N_C = 3$   $f_0(600)$  resonance completely disappears at large  $N_C$  or if it has a subdominant component in its structure, which would become dominant when the number of colors gets sufficiently high. Unfortunately, this depends on the chosen procedure ( $A, B.1$  and  $B.3$  or  $B.2$  and  $B.1-2$ ) to fit the phase-shift data. However, it becomes clear the predominant di-pion component of this pole for  $N_C = 3$ , and that the SRA delta-function-like pole, that always appears in the  $N_C \gg 1$

limit, might help to keep the whole scheme compatible with semilocal duality. Nevertheless, this needs to be quantitatively checked elsewhere.

## ACKNOWLEDGMENTS

We thank J.R. Peláez, J. Ruiz de Elvira and J.J. Sanz-Cillero for useful communications. This research was supported by DGI and FEDER funds, under Contract Nos. FIS2008-01143/FIS, FPA2007-60323, and the Spanish Consolider-Ingenio 2010 Programme CPAN (CSD2007-00042), by Junta de Andalucía Contract No. FQM0225, by Generalitat Valenciana under Contract Nos. PROMETEO/2008/069 and PROMETEO/2009/0090, and it is part of the European Community-Research Infrastructure Integrating Activity ‘‘Study of Strongly Interacting Matter’’ (acronym HadronPhysics2, Grant Agreement No. 227431), under the Seventh EU Framework Programme. A.P. acknowledges the support of the Alexander von Humboldt Foundation.

## APPENDIX A: GENERAL FEATURES OF $\pi\pi$ SCATTERING

A comprehensive presentation of  $\pi\pi$  scattering can be seen at the textbook level [69] and more recently in [70]. We summarize here some relevant formulae to provide a proper perspective of our analysis merging large  $N_C$ , ChPT and unitarity considerations.

With the conventions used in this work, the optical theorem reads

$$\sigma_I(s) = -\frac{1}{s\rho(s)} \text{Im}T_I(s, 0, 4m_\pi^2 - s) = \sum_J \sigma_{IJ}(s), \quad (\text{A1})$$

where the partial-wave total cross section is defined as

$$\begin{aligned} \sigma_{IJ}(s) &= 16\pi \frac{(2J+1)}{s-4m_\pi^2} \left[ \eta_{IJ} \sin^2 \delta_{IJ} + \frac{1}{2}(1-\eta_{IJ}) \right] \\ &\leq 8\pi(2J+1) \frac{1+\eta_{IJ}}{s-4m_\pi^2}. \end{aligned} \quad (\text{A2})$$

The contribution of a resonance state, with spin  $J$  and isospin  $I$ , to the partial cross section in the narrow-width limit and assuming  $m_{IJ}^2 \gg 4m_\pi^2$ , reads

$$\sigma_{IJ}(s) = (2J+1) \frac{16\pi^2 \Gamma_{IJ}}{m_{IJ}} \delta(s - m_{IJ}^2). \quad (\text{A3})$$

Of course, one may think that such a limit does not apply to a broad state as the  $\sigma$ . Within a Breit-Wigner model, the finite width correction effectively corresponds to a reduction  $\Gamma \rightarrow \Gamma[1 - \Gamma/(\pi m)]$ , which even for the extreme case  $\Gamma = m$  yields to a moderate 30% correction.

Up to  $\sqrt{s} \leq 1.4$  GeV, the S0, P, and D0 waves play an outstanding role [44] featuring the appearance of the  $f_0(600)$ ,  $\rho_1(770)$ ,  $f_0(980)$  and  $f_2(1270)$  resonances, while below the  $\bar{K}K$  production threshold,  $s_{\bar{K}K} = 4m_K^2$ , only S0 and P are essential.

### 1. Crossing and forward dispersion relations

In the (crossed)  $t$ -channel, the amplitudes read

$$\begin{pmatrix} T_{I_t=0}(s, t, u) \\ T_{I_t=1}(s, t, u) \\ T_{I_t=2}(s, t, u) \end{pmatrix} = \begin{pmatrix} \frac{1}{3} & 1 & \frac{5}{3} \\ \frac{1}{3} & \frac{1}{2} & -\frac{5}{6} \\ \frac{1}{3} & -\frac{1}{2} & \frac{1}{6} \end{pmatrix} \begin{pmatrix} T_{I_s=0}(s, t, u) \\ T_{I_s=1}(s, t, u) \\ T_{I_s=2}(s, t, u) \end{pmatrix}, \quad (\text{A4})$$

where  $I_t$  and  $I_s$  are the corresponding isospins in the  $t$ - and  $s$ -channels, respectively.

The rigorous Froissart bound from axiomatic field theory requires that in the forward direction ( $t = 0$ ) these amplitudes, up to logarithmic corrections, are asymptotically polynomially bound by a single power of  $s$ . Actually, in terms of the crossing-odd variable  $\nu = (s - u)/2$ , the amplitude  $T_{I_t}(\nu, t) \equiv T_{I_t}(\nu + 2m_\pi^2 - t/2, t, -\nu + 2m_\pi^2 - t/2)$  satisfies  $T_{I_t}(-\nu, t) = (-1)^{I_t} T_{I_t}(\nu, t) \rightarrow \nu^{n_{I_t}}$ , with  $n_{I_t} \leq 1$  when  $\nu \rightarrow \infty$ . This means that a forward ( $t = 0$ ) once-subtracted dispersion relation is fulfilled, by considering a closed contour excluding the cuts  $-\infty < \nu < -2m_\pi^2$  and  $2m_\pi^2 < \nu < +\infty$ , where  $T(\nu + i0^+) - T(\nu - i0^+) = 2i\text{Im}T(\nu + i0^+) \equiv 2i\text{Im}T(\nu)$ . The subtraction constant can be fixed at low energies, and more specifically at  $\nu = 0$  or equivalently  $s = 2m_\pi^2$ , i.e. below threshold. Thus, at  $t = 0$ , we get the forward dispersion relations (FDRs):

$$\begin{aligned} T_{I_t=0}(\nu, 0) &= T_{I_t=0}(0, 0) + \frac{2\nu^2}{\pi} \int_{2m_\pi^2}^{\infty} \frac{d\nu'}{\nu'} \frac{\text{Im}T_{I_t=0}(\nu', 0)}{\nu'^2 - \nu^2}, \\ \frac{T_{I_t=1}(\nu, 0)}{\nu} &= \lim_{\nu_0 \rightarrow 0} \frac{T_{I_t=1}(\nu_0, 0)}{\nu_0} + \frac{2\nu^2}{\pi} \int_{2m_\pi^2}^{\infty} \frac{d\nu'}{\nu'^2} \\ &\quad \times \frac{\text{Im}T_{I_t=1}(\nu', 0)}{\nu'^2 - \nu^2}, \\ T_{I_t=2}(\nu, 0) &= T_{I_t=2}(0, 0) + \frac{2\nu^2}{\pi} \int_{2m_\pi^2}^{\infty} \frac{d\nu'}{\nu'} \frac{\text{Im}T_{I_t=2}(\nu', 0)}{\nu'^2 - \nu^2}. \end{aligned} \quad (\text{A5})$$

The absorptive part of the amplitude can be written as an optical theorem in the  $\nu$  variable:

$$\text{Im}T_{I_t}(\nu, 0) = -\sqrt{\nu^2 - 4m_\pi^4} \sigma_{I_t}(\nu), \quad (\text{A6})$$

where one goes from  $I_t$  to  $I_s$  with the same  $s$ - $t$  crossing matrix as for the amplitudes, see Eq. (A4). The FDRs converge, provided  $|\text{Im}T_{I_t}(\nu, 0)| < \nu^a$  with  $a < 2$ , for large values of  $\nu$ . Results for  $\sigma_{I_t}$  are presented in Fig. 6, up to  $\sqrt{s} = 1.42$  GeV, using the UFD parameterization of Ref. [44] for the partial S, P, D, and F waves

These general constraints are obeyed for any Quantum Field Theory and by QCD, in particular. On the other hand, for  $t \neq 0$ , and sufficiently large  $\nu$ , say  $\nu > \nu_h$ , one has the phenomenologically successful Regge behavior given by<sup>18</sup>

<sup>18</sup>Our amplitude and that used ( $F(\nu, t)$ ) in Ref. [44] are related by  $T(\nu, t) = -2\pi^2 F(\nu, t)$ .

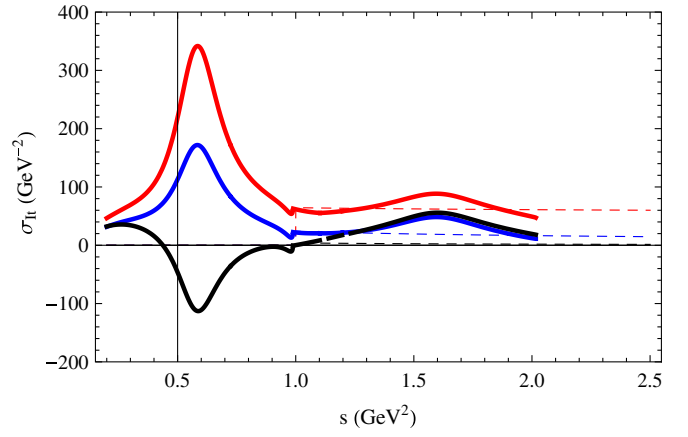


FIG. 6 (color online). The  $I_t = 0, 1, 2$  total cross sections, as a function of the  $s$  variable, including S, P, D, and F waves below  $\sqrt{s} = 1.42$  GeV (solid lines) and the corresponding Regge behavior starting at  $\sqrt{s} = 1.42$  GeV (dashed lines) used in the solutions of Ref. [44].  $I_t = 0$  (Red),  $I_t = 1$  (Blue) and  $I_t = 2$  (Black).

$$\text{Im}T_{I_t}(\nu, t) \rightarrow -2\pi^2 \sum \beta_{I_t}(t) \left[ \frac{\nu}{\nu_0} \right]^{\alpha_{I_t}(t)}, \quad (\text{A7})$$

where  $\sum$  indicates summation over several Regge trajectories, which for small  $t$  are given by  $\alpha_{I_t}(t) = \alpha_{I_t}(0) + t\alpha'_{I_t} + \dots$ . The slope parameter,  $\alpha'_{I_t}(0) \sim 1/(2m_\rho^2) = 0.9\text{GeV}^{-2}$  is nearly universal and the leading trajectory intercepts are  $\alpha_0(0) \sim 1$ ,  $\alpha_1(0) \sim 1/2$ , and  $\alpha_2(0) \sim 0$  (for a review within a modern  $\pi\pi$  context see e.g. Refs. [71,72] and references therein). We also show in Fig. 6 the Regge behavior used in the construction of the partial waves via FDRs, Roy and GKPY equations.<sup>19</sup> As we see, there is some mismatch between the partial waves and the Regge behavior. This is somewhat expected, since Regge behavior provides an average of the oscillating resonance contribution in the high-energy region. The region  $\sqrt{s} < 1.42$  GeV is well described by S, P, D, and F waves, since the exchanged  $\rho$  meson in the  $t$ -channel corresponds to longest range  $1/m_\rho$  and hence  $J_{\text{max}} \sim \sqrt{s}/m_\rho$ .

### 2. Finite energy sum rules

Separating the Regge tail in the dispersive integral, corresponding to the integration region  $\nu' > \nu_h$ , we have for  $I_t = 0, 2$ , in the limit  $\nu \rightarrow +\infty$  and assuming  $\alpha_{I_t}(0) < 2$ ,

<sup>19</sup>For our purposes we need the following Regge tails [44], valid for  $s > s_h = (1.42 \text{ GeV})^2$ :

$$\begin{aligned} \text{Im}T_{I_t=0}(\nu, 0) &= -2\pi^2 [b_P(\nu/\nu_0) + b_{P'}(\nu/\nu_0)^{a_{P'}}], \\ \text{Im}T_{I_t=1}(\nu, 0) &= -2\pi^2 b_1(\nu/\nu_0)^{a_1}, \\ \text{Im}T_{I_t=2}(\nu, 0) &= -2\pi^2 b_2(\nu/\nu_0)^{a_2}. \end{aligned} \quad (\text{A8})$$

The numerical values of the parameters are given in Sec. 8 of Appendix A of Ref. [44].

$$\begin{aligned}
 T_{I_t}(\nu, 0)|_{\text{Regge}} &\equiv \frac{2\nu^2}{\pi} \int_{\nu_h}^{\infty} \frac{d\nu'}{\nu'} \\
 &\times \frac{[-2\pi^2 \sum \beta_{I_t}(0)(\nu'/\nu_0)^{\alpha_{I_t}(0)}]}{\nu'^2 - \nu^2 - i\epsilon} \\
 &= 2\pi^2 \sum \frac{\beta_{I_t}(0)}{\sin(\frac{\alpha_{I_t}(0)\pi}{2})} e^{-i\alpha_{I_t}(0)\pi/2} \left(\frac{\nu}{\nu_0}\right)^{\alpha_{I_t}(0)} \\
 &\quad - 4\pi \sum \frac{\beta_{I_t}(0)}{\alpha_{I_t}(0)} \left(\frac{\nu_h}{\nu_0}\right)^{\alpha_{I_t}(0)} + \mathcal{O}(\nu_0/\nu)
 \end{aligned} \tag{A9}$$

and similarly for  $I_t = 1$ ,

$$\begin{aligned}
 \frac{T_{I_t=1}(\nu, 0)}{\nu}|_{\text{Regge}} &\equiv \frac{2\nu^2}{\pi} \int_{\nu_h}^{\infty} \frac{d\nu'}{\nu'^2} \frac{[-2\pi^2 \sum \beta_{I_t=1}(0)(\nu'/\nu_0)^{\alpha_{I_t=1}(0)}]}{\nu'^2 - \nu^2 - i\epsilon} \\
 &= \left(2\pi^2 \sum \frac{\beta_{I_t=1}(0)}{\sin(\frac{\hat{\alpha}\pi}{2})} e^{-i\hat{\alpha}\pi/2} \left(\frac{\nu}{\nu_0}\right)^{\hat{\alpha}}\right. \\
 &\quad \left. - 4\pi \sum \frac{\beta_{I_t=1}(0)}{\hat{\alpha}} \left(\frac{\nu_h}{\nu_0}\right)^{\hat{\alpha}}\right) \frac{1}{\nu_0} + \mathcal{O}(1/\nu),
 \end{aligned} \tag{A10}$$

with  $\hat{\alpha} = \alpha_{I_t=1}(0) - 1$ . Note that the last term in both Eqs. (A9) and (A10) is a constant subleading contribution. We will denote this constant term as  $-R_{I_t}$ . Requiring

$$\begin{aligned}
 T_{I_t}(\nu, 0) &\rightarrow 2\pi^2 \sum \frac{\beta_{I_t}(0)}{\sin(\frac{\alpha_{I_t}(0)\pi}{2})} e^{-i\alpha_{I_t}(0)\pi/2} \left(\frac{\nu}{\nu_0}\right)^{\alpha_{I_t}(0)}, \\
 I_t &= 0, 2,
 \end{aligned} \tag{A11}$$

$$\frac{T_{I_t=1}(\nu, 0)}{\nu} \rightarrow \frac{2\pi^2}{\nu_0} \sum \frac{\beta_{I_t=1}(0)}{\sin(\frac{\hat{\alpha}\pi}{2})} e^{-i\hat{\alpha}\pi/2} \left(\frac{\nu}{\nu_0}\right)^{\hat{\alpha}}, \tag{A12}$$

in the  $\nu \rightarrow +\infty$  limit, we get the finite energy sum rules

$$\begin{aligned}
 T_{I_t=0}(0) &= -\frac{2}{\pi} \int_{2m_\pi^2}^{\nu_h} d\nu \sqrt{1 - \frac{4m_\pi^4}{\nu^2}} \sigma_{I_t=0}(\nu) + R_{I_t=0}, \\
 T'_{I_t=1}(0) &= -\frac{2}{\pi} \int_{2m_\pi^2}^{\nu_h} \frac{d\nu}{\nu} \sqrt{1 - \frac{4m_\pi^4}{\nu^2}} \sigma_{I_t=1}(\nu) + R'_{I_t=1}, \\
 T_{I_t=2}(0) &= -\frac{2}{\pi} \int_{2m_\pi^2}^{\nu_h} d\nu \sqrt{1 - \frac{4m_\pi^4}{\nu^2}} \sigma_{I_t=2}(\nu) + R_{I_t=2},
 \end{aligned} \tag{A13}$$

where

$$\begin{aligned}
 R_{I_t=0} &= 4\pi b_P \left(\frac{\nu_h}{\nu_0}\right) + 4\pi \frac{b_{P'}}{a_{P'}} \left(\frac{\nu_h}{\nu_0}\right)^{a_{P'}}, \\
 R'_{I_t=1} &= \frac{4\pi b_1}{a_1 - 1} \frac{1}{\nu_h} \left(\frac{\nu_h}{\nu_0}\right)^{a_1}, \\
 R_{I_t=2} &= 4\pi \frac{b_2}{a_2} \left(\frac{\nu_h}{\nu_0}\right)^{a_2}.
 \end{aligned} \tag{A14}$$

For  $\sqrt{s_h} = \sqrt{\nu_h + 2m_\pi^2} = 1.42$  GeV, we get the values  $T_{I_t=0}(0) = -121.8 + 64.3(P) + 28.2(P') = -29.3$ ,  $T'_{I_t=1}(0) = -105.2 - 19.4(\rho)$  GeV<sup>-2</sup> = -124.6 GeV<sup>-2</sup> and  $T_{I_t=2}(0) = -12.25 + R_{I_t=2}$ . Indeed, in the window  $\sqrt{\nu_h} \in (1, 1.42)$  GeV, we observe a smooth  $\nu_h$  dependence of both the integral and the  $R_{I_t}$  contributions.<sup>20</sup> Moreover, the total sum itself remains fairly independent of  $\nu_h$ , as well. Being more quantitative, the right-hand side of Eqs. (A13) changes at the level of 10% and 4% for the  $I_t = 0$  and 1 cases, respectively, when  $\sqrt{\nu_h}$  varies in the interval (1,1.42) GeV. For the case  $I_t = 1$ ,  $R'_{I_t=1}$  amounts, at energies as small as 1 GeV, to around 25% of the total, and decreases with increasing  $\nu_h$ , as deduced from its Regge behavior. For the case of  $I_t = 2$ , the integral contribution shows a more pronounced dependence on  $\nu_h$ , and it changes sign at around half of the (1,1.42) GeV interval. However, this contribution in size is just at maximum around one third of that of  $R_{I_t=2}$ , which is almost constant, because of the smallness of the Regge intercept,  $a_2$ . Furthermore, the sign of  $R_{I_t=2}$  depends on the sign of  $a_2$  and actually the finite energy sum rule becomes ambiguous for  $a_2 = 0$ , since the amplitude would show a logarithmic growth  $\sim \log(-\nu^2/\nu_h^2)$  instead of a Regge behavior. For a diverging/converging amplitude we have a positive/negative contribution to the sum rule. These ambiguous signs appear in the CFD and UFD solutions of Ref. [44], from where one gets  $R_{I_t=2} = -30(30)$  and  $R_{I_t=2} = 20(40)$ , respectively, both results compatible with zero.

### 3. Adler and $\sigma$ sum rules

If  $R'_{I_t=1}$  and  $R_{I_t=2}$  are neglected in Eqs. (A13), as suggested by the numerical values obtained from the fits performed in Ref. [44], and  $T'_{I_t=1}(0)$  and  $T_{I_t=2}(0)$  are approximated by the lowest-order result in ChPT, see Eq. (A15) below, the so-called Adler and  $\sigma$  sum rules (see e.g. [69] for a discussion based on current algebra and PCAC) are obtained when in addition  $\nu_h \rightarrow \infty$ <sup>21</sup>

<sup>20</sup>We use the UFD parameterization of Ref. [44].

<sup>21</sup>The corresponding  $\nu = 0$   $t$ -channel forward scattering amplitudes at one loop are given by

$$\begin{aligned}
 T_{I_t=0}(0) &= \frac{m_\pi^2}{2f_\pi^2} + \frac{m_\pi^4(-72\bar{l}_1 - 48\bar{l}_2 + 45\bar{l}_3 + 36\bar{l}_4 + 39\pi - 101)}{576\pi^2 f_\pi^4} \\
 &\quad + \mathcal{O}(p^6), \\
 T'_{I_t=1}(0) &= -\frac{1}{f_\pi^2} + \frac{(-48\bar{l}_4 + 9\pi - 10)m_\pi^2}{384\pi^2 f_\pi^4} + \mathcal{O}(p^6), \\
 T_{I_t=2}(0) &= -\frac{m_\pi^2}{f_\pi^2} + \frac{(-48\bar{l}_2 + 18\bar{l}_3 - 72\bar{l}_4 + 21\pi + 10)m_\pi^4}{576\pi^2 f_\pi^4} \\
 &\quad + \mathcal{O}(p^6).
 \end{aligned} \tag{A15}$$

The  $\mathcal{O}(p^4)$  corrections are at the 10–20% level of the lowest-order ones in the Adler and  $\sigma$  sum rules.

$$\frac{1}{f_\pi^2} = \frac{2}{\pi} \int_{2m_\pi^2}^{\infty} \frac{d\nu}{\nu} \sqrt{1 - \frac{4m_\pi^4}{\nu^2}} \left[ \frac{1}{3} \sigma_0(\nu) + \frac{1}{2} \sigma_1(\nu) - \frac{5}{6} \sigma_2(\nu) \right], \quad (\text{A16})$$

$$\frac{m_\pi^2}{f_\pi^2} = \frac{2}{\pi} \int_{2m_\pi^2}^{\infty} d\nu \sqrt{1 - \frac{4m_\pi^4}{\nu^2}} \left[ \frac{1}{3} \sigma_0(\nu) - \frac{1}{2} \sigma_1(\nu) + \frac{1}{6} \sigma_2(\nu) \right], \quad (\text{A17})$$

Using the GKPRY parameterizations [44], one finds that the contribution of the region  $\nu > 1.42$  GeV, for which Regge behavior is assumed, is quite small. This is because  $\sigma_{I_t}(\nu) \rightarrow 4\pi^2 \beta_{I_t}(0) \nu^{\alpha_{I_t}(0)-1}$ . In addition, we would like to point out

- (i)  $I_t = 1$ : Following the discussion of the previous section, neglecting the contribution to the sum rule arising from the region  $\sqrt{\nu} \in (1, 1.4)$  GeV might induce variations of order 20%, which we expect to be of the same order as those stemming from  $\mathcal{O}(p^4)$  ChPT terms neglected in the left-hand side of the sum rule. The Adler sum rule is satisfied to 5% (see also [73]) in the partial-wave plus Regge representation.
- (ii)  $I_t = 2$ : This sum rule converges if  $\alpha_{I_t=2}(0) < 0$  and is the  $\sigma$  sum rule derived in [69] on the basis of PCAC. The  $\sigma$  sum rule is already approximately satisfied for an upper limit of the integration around  $\sqrt{s} < 1.26$  GeV. The contribution above this upper limit tends to cancel and shows an oscillating behavior as a function of the upper limit of the integration. This is closely linked with having a value of  $b_2$  compatible with zero and a not well-defined sign for the ratio  $b_2/a_2$  appearing in  $R_{I_t=2}$ . For an upper limit of  $\sqrt{s} < 1.26$ , the truncated Adler sum rule also provides a rather reasonable value of 89 MeV for  $f_\pi$ . This result is certainly more reasonable if one bears in mind that the left-hand side of the sum rule has been computed at lowest order in ChPT only. This observation suggests a kind of superconvergent dispersion relation which will be important to set up our model below.

Given the above discussion, one finds reasons to saturate the sum rules with the lowest-lying resonances below 1 GeV. In addition, we already mentioned that the  $I_t = 0$  sum rule in Eq. (A13) is saturated also, with great accuracy, at 1 GeV (integral and  $R$  contributions tend to cancel above 1 GeV). All this, gives support to the scenarios assumed in this work, where we have taken into account only the lowest-lying resonance degrees of freedom. Yet, we will make use of the Adler and  $\sigma$  sum rules, saturated at energies of about 1 GeV, to find out short-distance constraints that will make more predictive the  $R\chi T$  approach adopted here.

## APPENDIX B: SU(2) AND SU(3) CHPT $\pi\pi$ SCATTERING

For the sake of completeness, we recall here the relation between the LECs  $\bar{l}_i$  and the most common SU(3) parameters  $L_i^r(\mu)$  [12,13]:

$$\bar{l}_i = \frac{32\pi^2}{\gamma_i} l_i^r(\mu) - \log(m_\pi^2/\mu^2), \quad \gamma_1 = \frac{1}{3}, \quad (\text{B1})$$

$$\begin{aligned} \gamma_2 &= \frac{2}{3}, & \gamma_3 &= -\frac{1}{2}, & \gamma_4 &= 2 \\ l_1^r &= 4L_1^r + 2L_3 - \frac{\nu_K}{24}, & l_2^r &= 4L_2^r - \frac{\nu_K}{12}, \\ l_3^r &= -8L_4^r - 4L_5^r + 16L_6^r + 8L_8^r - \frac{\nu_\eta}{18}, & & \\ l_4^r &= 8L_4^r + 4L_5^r - \frac{\nu_K}{2}, & & \end{aligned} \quad (\text{B2})$$

with  $32\pi^2 \nu_{K,\eta} = 1 + \log(\hat{m}_{K,\eta}^2/\mu^2)$ ,  $\hat{m}_\eta = 4\hat{m}_K/3$  and  $\hat{m}_K \sim 468$  GeV the kaon mass in the limit  $m_u = m_d = 0$ . The renormalized coupling constants  $l_i^r(\mu)$  and  $L_i^r(\mu)$  depend logarithmically on the dimensional regularization scale  $\mu$ :

$$L_i^r(\mu_2) = L_i^r(\mu_1) + \frac{\Gamma_i}{16\pi^2} \log\left(\frac{\mu_1}{\mu_2}\right), \quad (\text{B3})$$

where  $\Gamma_1 = 3/32$ ,  $\Gamma_2 = 3/16$ ,  $\Gamma_3 = 0$ ,  $\Gamma_4 = 1/8$ ,  $\Gamma_5 = 3/8$ ,  $\Gamma_6 = 11/144$ ,  $\Gamma_8 = 5/48$ .

On the other hand,  $A_4^{\text{SRA}}$  in Eq. (23) can be rewritten as

$$\begin{aligned} A_4^{\text{SRA}}(s, t, u) &= \frac{m_\pi^2 - s}{f_\pi^2} - \frac{4}{f_\pi^4} \left\{ (2L_1^{\text{SRA}} + L_3^{\text{SRA}})(s - 2m_\pi^2)^2 \right. \\ &\quad \left. + L_2^{\text{SRA}}[(t - 2m_\pi^2)^2 + (u - 2m_\pi^2)^2] \right\} \\ &\quad - \frac{8m_\pi^2}{f_\pi^4} \left\{ (2L_4^{\text{SRA}} + L_5^{\text{SRA}})s \right. \\ &\quad \left. + (4L_6^{\text{SRA}} + 2L_8^{\text{SRA}} - 4L_4^{\text{SRA}} - 2L_5^{\text{SRA}})m_\pi^2 \right\}. \end{aligned} \quad (\text{B4})$$

From Eqs. (23) and (17), one trivially finds

$$\begin{aligned} 2L_1^{\text{SRA}} = L_2^{\text{SRA}} &= \frac{f_\pi^2}{8m_V^2}, & L_3^{\text{SRA}} &= -\frac{3f_\pi^2}{8m_V^2} + \frac{f_\pi^2}{8m_S^2}, \\ L_4^{\text{SRA}} &= 0, & L_5^{\text{SRA}} &= \frac{f_\pi^2}{4m_S^2}, & L_6^{\text{SRA}} &= 0, \\ L_8^{\text{SRA}} &= \frac{3f_\pi^2}{32m_S^2}, & & & & \end{aligned} \quad (\text{B5})$$

in full agreement with Ref. [18].<sup>22</sup>

<sup>22</sup>If the relation  $m_S = m_V$  is further assumed, one gets purely geometrical ratios for the nonvanishing LECs:

$$2L_1^{\text{SRA}} = L_2^{\text{SRA}} = -\frac{1}{2}L_3^{\text{SRA}} = \frac{1}{2}L_5^{\text{SRA}} = \frac{4}{3}L_8^{\text{SRA}} = \frac{f_\pi^2}{8m_V^2}.$$

In chiral quark models with meson dominance built in, one also has  $m_S = m_V = \sqrt{24/N_C} \pi f \sim 781$  GeV, for  $f = 88$  GeV [49], so that the above relations hold with  $L_2 = N_C/192\pi^2 = 1.5 \times 10^{-3}$ .

- [1] M.H. Johnson and E. Teller, *Phys. Rev.* **98**, 783 (1955).
- [2] I. Caprini, G. Colangelo, and H. Leutwyler, *Phys. Rev. Lett.* **96**, 132001 (2006).
- [3] R. Kaminski, J. R. Pelaez, and F. J. Yndurain, *Phys. Rev. D* **77**, 054015 (2008).
- [4] R. Garcia-Martin, R. Kaminski, J. R. Pelaez, and J. Ruiz de Elvira, *Phys. Rev. Lett.* **107**, 072001 (2011).
- [5] E. Klempt and A. Zaitsev, *Phys. Rep.* **454**, 1 (2007).
- [6] J. R. Pelaez, *Phys. Rev. Lett.* **92**, 102001 (2004).
- [7] G. 't Hooft, *Nucl. Phys.* **B72**, 461 (1974).
- [8] E. Witten, *Nucl. Phys.* **B160**, 57 (1979).
- [9] G. Ecker, J. Gasser, A. Pich, and E. de Rafael, *Nucl. Phys.* **B321**, 311 (1989).
- [10] G. Ecker, J. Gasser, H. Leutwyler, A. Pich, and E. de Rafael, *Phys. Lett. B* **223**, 425 (1989).
- [11] S. Weinberg, *Physica A (Amsterdam)* **96**, 327 (1979).
- [12] J. Gasser and H. Leutwyler, *Ann. Phys. (N.Y.)* **158**, 142 (1984).
- [13] J. Gasser and H. Leutwyler, *Nucl. Phys.* **B250**, 465 (1985).
- [14] V. Cirigliano *et al.*, *Nucl. Phys.* **B753**, 139 (2006).
- [15] J. Bijnens, E. Gamiz, E. Lipartia, and J. Prades, *J. High Energy Phys.* **04** (2003) 055.
- [16] F. Sannino and J. Schechter, *Phys. Rev. D* **52**, 96 (1995).
- [17] M. Harada, F. Sannino, and J. Schechter, *Phys. Rev. D* **54**, 1991 (1996).
- [18] A. Pich, [arXiv:hep-ph/0205030](https://arxiv.org/abs/hep-ph/0205030).
- [19] J. Nieves and E. Ruiz Arriola, *Phys. Lett. B* **679**, 449 (2009).
- [20] J. Nebreda, J. R. Pelaez, and G. Rios, *Phys. Rev. D* **84**, 074003 (2011).
- [21] Z. X. Sun, L. Y. Xiao, Z. Xiao, and H. Q. Zheng, *Mod. Phys. Lett. A* **22**, 711 (2007).
- [22] J. R. Pelaez and G. Rios, *Phys. Rev. Lett.* **97**, 242002 (2006).
- [23] J. Nieves and E. R. Arriola, *Phys. Rev. D* **80**, 045023 (2009).
- [24] P. Di Vecchia and G. Veneziano, *Nucl. Phys.* **B171**, 253 (1980).
- [25] E. Witten, *Ann. Phys. (N.Y.)* **128**, 363 (1980).
- [26] C. Rosenzweig, J. Schechter, and C. Trahern, *Phys. Rev. D* **21**, 3388 (1980).
- [27] R. Kaiser and H. Leutwyler, *Eur. Phys. J. C* **17**, 623 (2000).
- [28] N. Beisert and B. Borasoy, *Phys. Rev. D* **67**, 074007 (2003).
- [29] M. Albaladejo, J. A. Oller, and L. Roca, *Phys. Rev. D* **82**, 094019 (2010).
- [30] Z.-H. Guo and J. Oller, *Phys. Rev. D* **84**, 034005 (2011).
- [31] J. Ruiz de Elvira, J. R. Pelaez, M. R. Pennington, and D. J. Wilson, [arXiv:1009.6204](https://arxiv.org/abs/1009.6204).
- [32] J. Nieves and E. Ruiz Arriola, *Nucl. Phys.* **A679**, 57 (2000).
- [33] D. Black, A. H. Fariborz, F. Sannino, and J. Schechter, *Phys. Rev. D* **59**, 074026 (1999).
- [34] V. Cirigliano, G. Ecker, H. Neufeld, and A. Pich, *J. High Energy Phys.* **06** (2003) 012.
- [35] F. Giacosa, T. Gutsche, V. E. Lyubovitskij, and A. Faessler, *Phys. Rev. D* **72**, 094006 (2005).
- [36] Z.-H. Guo and J. J. Sanz-Cillero, *Phys. Rev. D* **79**, 096006 (2009).
- [37] Z. H. Guo, J. J. Sanz Cillero, and H. Q. Zheng, *J. High Energy Phys.* **06** (2007) 030.
- [38] A. Pich, I. Rosell, and J. J. Sanz-Cillero, *J. High Energy Phys.* **02** (2011) 109.
- [39] Z.-H. Guo and P. Roig, *Phys. Rev. D* **82**, 113016 (2010).
- [40] G. Ecker, *Acta Phys. Pol. B* **38**, 2753 (2007).
- [41] F. J. Gilman and H. Harari, *Phys. Rev.* **165**, 1803 (1968).
- [42] S. Weinberg, *Phys. Rev.* **177**, 2604 (1969).
- [43] S. Weinberg, *Phys. Rev. Lett.* **65**, 1177 (1990).
- [44] R. Garcia-Martin, R. Kaminski, J. Pelaez, J. Ruiz de Elvira, and F. Yndurain, *Phys. Rev. D* **83**, 074004 (2011).
- [45] G. Ecker and C. Zauner, *Eur. Phys. J. C* **52**, 315 (2007).
- [46] D. Toublan, *Phys. Rev. D* **53**, 6602 (1996).
- [47] K. Nakamura *et al.*, *J. Phys. G* **37**, 075021 (2010).
- [48] C. Garcia-Recio, L. Geng, J. Nieves, and L. Salcedo, *Phys. Rev. D* **83**, 016007 (2011).
- [49] E. Megias, E. Ruiz Arriola, L. L. Salcedo, and W. Broniowski, *Phys. Rev. D* **70**, 034031 (2004).
- [50] J. Nieves and E. Ruiz Arriola, *Phys. Lett. B* **455**, 30 (1999).
- [51] I. Rosell, J. J. Sanz-Cillero, and A. Pich, *J. High Energy Phys.* **08** (2004) 042.
- [52] I. Rosell, J. J. Sanz-Cillero, and A. Pich, *J. High Energy Phys.* **01** (2007) 039.
- [53] A. Pich, I. Rosell, and J. J. Sanz-Cillero, *J. High Energy Phys.* **07** (2008) 014.
- [54] I. Rosell, P. Ruiz-Femenia, and J. Portoles, *J. High Energy Phys.* **12** (2005) 020.
- [55] J. Portoles, I. Rosell, and P. Ruiz-Femenia, *Phys. Rev. D* **75**, 114011 (2007).
- [56] J. Nieves and E. Ruiz Arriola, *Phys. Rev. D* **64**, 116008 (2001).
- [57] B. Ananthanarayan, G. Colangelo, J. Gasser, and H. Leutwyler, *Phys. Rep.* **353**, 207 (2001).
- [58] F. J. Yndurain, R. Garcia-Martin, and J. R. Pelaez, *Phys. Rev. D* **76**, 074034 (2007).
- [59] P. Estabrooks and A. D. Martin, *Nucl. Phys.* **B79**, 301 (1974).
- [60] S. D. Protopopescu *et al.*, *Phys. Rev. D* **7**, 1279 (1973).
- [61] W. Hoogland *et al.*, *Nucl. Phys.* **B126**, 109 (1977).
- [62] M. Losty, V. Chaloupka, A. Ferrando, L. Montanet, E. Paul, D. Yaffe, J. Zieminski *et al.*, *Nucl. Phys.* **B69**, 185 (1974), ISSN .
- [63] G. Amoros, J. Bijnens, and P. Talavera, *Nucl. Phys.* **B585**, 293 (2000).
- [64] J. Bernabeu and J. Prades, *Phys. Rev. Lett.* **100**, 241804 (2008).
- [65] H. Leutwyler, *AIP Conf. Proc.* **1030**, 46 (2008).
- [66] Z.-Y. Zhou and Z. Xiao, *Phys. Rev. D* **83**, 014010 (2011).
- [67] N. A. Tornqvist, *Z. Phys. C* **68**, 647 (1995).
- [68] E. Ruiz Arriola and W. Broniowski, *Phys. Rev. D* **81**, 054009 (2010).
- [69] B. Martin, D. Morgan, and G. Shaw, *Pion-Pion Interactions in Particle Physics* (Academic Press, London, 1976), Vol. 101.
- [70] F. J. Yndurain, [arXiv:hep-ph/0212282](https://arxiv.org/abs/hep-ph/0212282).
- [71] J. R. Pelaez and F. J. Yndurain, *Phys. Rev. D* **68**, 074005 (2003).
- [72] J. R. Pelaez and F. J. Yndurain, *Phys. Rev. D* **69**, 114001 (2004).
- [73] S. L. Adler and F. J. Yndurain, *Phys. Rev. D* **75**, 116002 (2007).